Quaternary Science Reviews 361 (2025) 109404

Contents lists available at ScienceDirect

Quaternary Science Reviews

journal homepage: www.elsevier.com/locate/quascirev

Geomorphology, first ^{36}Cl datings and chrono-evolutionary model of Mount Aragats paleoglaciers (Armenia)

Carrasco R.M.[1], Fernández-Lozano J.[2], Karampaglidis T.[1], Soteres R.L.[3,4], Braucher R.[5], Gairoard S.[5], Petrosyan A.[6], Nahapetyan S.[6], Arakelyan D.[7], Pedraza J.[8], Gasparyan B.[6], ASTER Team, G. Aumaître[5], K. Keddadouche[5], F. Zaidi[5]

[1] Department of Geological and Mining Engineering, Castilla-La Mancha University, Toledo, Spain
[2] Department. of Mining, Topography and Structures Engineering, Universidad de León, Spain
[3] GAIA-Antártica Research Center, Universidad de Magallanes, Chile
[4] Cape Horn International Center (CHIC), Universidad de Magallanes, Chile
[5] CEREGE, Aix Marseille Univ., CNRS, IRD, INRAE, Collège de France, Aix-en-Provence, France
[6] Institute of Archaeology and Ethnography, National Academy of Sciences of the Republic of Armenia, Yerevan, Armenia
[7] Institute of Geological Sciences of the National Academy of Sciences of the Republic of Armenia, Yerevan, Armenia
[8] Department of Geodynamics, Stratigraphy and Paleontology, Complutense University, Madrid, Spain

ARTICLE INFO

Handling editor: Donatella Magri

Keywords:
Glaciovolcanic morphology
Aragats mountain
^{36}Cl-CRE dating
Penultimate glacial cycle
Last glacial cycle
Armenian highlands

ABSTRACT

Mount Aragats is one of the largest glaciated volcanoes of the Armenian Highlands (Հայկական լեռնաշխարհ) and culminating in the Aragats Peak, the highest peak of the Republic of Armenia (4090 masl). Here, prehistoric societies have been present for millennia, so assessing the local influence of past glaciations is a crucial factor to better understand the cultural evolution of this region. Therefore, this work focuses on a detailed study of the morphology and morphostratigraphic succession of Mount Aragats paleoglaciers. Geomorphic-based paleoglacier reconstruction along 36Cl cosmogenic dating (n = 13) of moraines reveal that during the Middle and Upper Pleistocene, a plateau glacier featuring ice lobes covered this area, featuring outlet lobes reaching up to 17 km in length, thicknesses of up to 350 m and descending to 2040 masl. According to the morphostratigraphic succession of ice-marginal features, absolute chronologies and regional correlations, the chronoevolutionary sequence of these glaciers comprises three intervals: (1) The absolute Maximum Ice Extent or Aragats Glacial Maximum occurred during the Penultimate Glacial Cycle within the MIS6e (c. 180 ka). (2) Subsequently, during the Last Glacial Cycle, the Maximum Ice Extent occurred during the MIS5d (c. 111 ka) followed by two secondary glacial maxima stabilizations during the MIS3a (c. 37 ka) and the MIS2 (c. 17 ka). Finally, (3) the Post-Glacial Period (PCP, Holocene, MIS1). The disappearance of the glaciers on Mount Aragats was established at the beginning of the second half of the 20th century by direct observations. The current morphodynamic environment corresponds to active rock glaciers, some névè moraines and widespread activity of slope processes such as debris flow and debris slides.

1. Introduction

Mount Aragats is located in a volcanic region that has had a remarkable historical, cultural, and architectural significance since prehistoric timesplaying a vital role in human development from the Palaeolithic to the Christian Era. The slopes of Mount Aragats preserve remnants of rock art, including paintings and engravings found on tuffs and basalts. These suitable rock surfaces served as locations for shelters during the transition from the Late Mesolithic to the Early Neolithic as well as Chalcolithic (Feruglio et al., 2005; Khechoyan et al., 2007; Arimura et al., 2012; Colonge et al., 2013; Petrosyan et al., 2014, 2021; Khechoyan and Gasparyan, 2014). Likewise, evidence of human occupation during the Bronze and Iron Ages exists around the entire sectors of Mount Aragats, supported by the presence of fortifications and burial sites, as well as kite structures and irrigation systems (Kalantar, 2003; Badalyan and Avetisyan, 2007; Lindsay and Smith, 2006; Nadel et al., 2015; Lindsay et al., 2022). Finally, during the Christian eras, the use of ignimbrites as building stones was widespread in cathedrals and

This article is part of a special issue entitled: Southern Caucasus published in Quaternary Science Reviews.

https://doi.org/10.1016/j.quascirev.2025.109404
Received 14 December 2024; Received in revised form 24 April 2025; Accepted 4 May 2025
Available online 14 May 2025

monasteries across the region.

Due to its geographical location in the North-eastern Armenian Highlands, Mount Aragats occupies a privileged local position for the study of the impact of regional climatic situations dominated by the westerly airflow in the transit of the W-E global circulation cells (Zhao et al., 2024). As a result, and as in the neighbouring lowlands of the southern Caucasian valleys, the Armenian Highland is a topographic corridor that facilitated hominin expansion from Asia Minor, Levant, and Arabian Peninsula into the rest of Eurasia during the Pleistocene (Loveluck et al., 2024; Wolf et al., 2024).

The Caucasus region forms part of the Alpine Mountain Belt and "is located in the transitional area between the Euro-Mediterranean and Asian climates with seasonal influences from the Westerlies, the Siberian High and far-reaching impacts from the Indian Summer Monsoon" (Joannin et al., 2014; Stockhecke et al., 2016; von Suchodoletz et al., 2018). Since glacial dynamics are sensitive to climate changes, reconstructing the structure and chronology of past glacial fluctuations allows the study of local-to-global climate variations far beyond the historical records and, thus, their impact on past population migration. Glacial activity during the Pleistocene and Holocene has been reported in several mountain areas of the Greater and Lesser Caucasus (Çiner, 2004; Sarikaya et al., 2011; Tielidze, 2017; Tielidze and Wheate, 2018; Revaz et al., 2018; Boynagryan, 2021; Solomina et al., 2022). However, the knowledge of glacier behaviour during past glaciations in the Mount Aragats region is still obscure, precluding assessment of how natural climate variability could influence early human populations.

This work aims to carry out a detailed geomorphological study of Mount Aragats emphasizing the identification and mapping of glacial landforms, particularly ice-marginal features, to provide the first absolute chronology based on ^{36}Cl Cosmic Ray Exposure dating (CRE) of the glacial activity during past glaciations in Mount Aragats area. Specifically, this work seeks to answer questions such as the timing of the maximum ice extent during past glaciations and the chronology of the last glaciation, including the onset of the last deglaciation. This information is the foundation for proposing a first-order chronoevolutionary sequence model for the Mount Aragats glaciations.

In addition, Mount Aragats past glaciations evolution is correlated with other areas at local and regional scales to contextualise Quaternary glaciations at hemispheric scale. The analyzed paleoenvironmental variables provide new insights into the interactions between environmental changes, glacial processes, and human adaptation in a dynamic highland environment.

2. Geological and geomorphological framework

Since the early geological studies conducted in historical Armenia by the German geologist Hermann Abich (1882) and Felix Oswald (1906), who provided some of the first detailed geological sections of the country, a solid foundation was established in the areas of tectonics and volcanism that have served for future research.

The Republic of Armenia is situated in the central part of the Arabia-Eurasia collision zone across the so-called Armenian Highlands

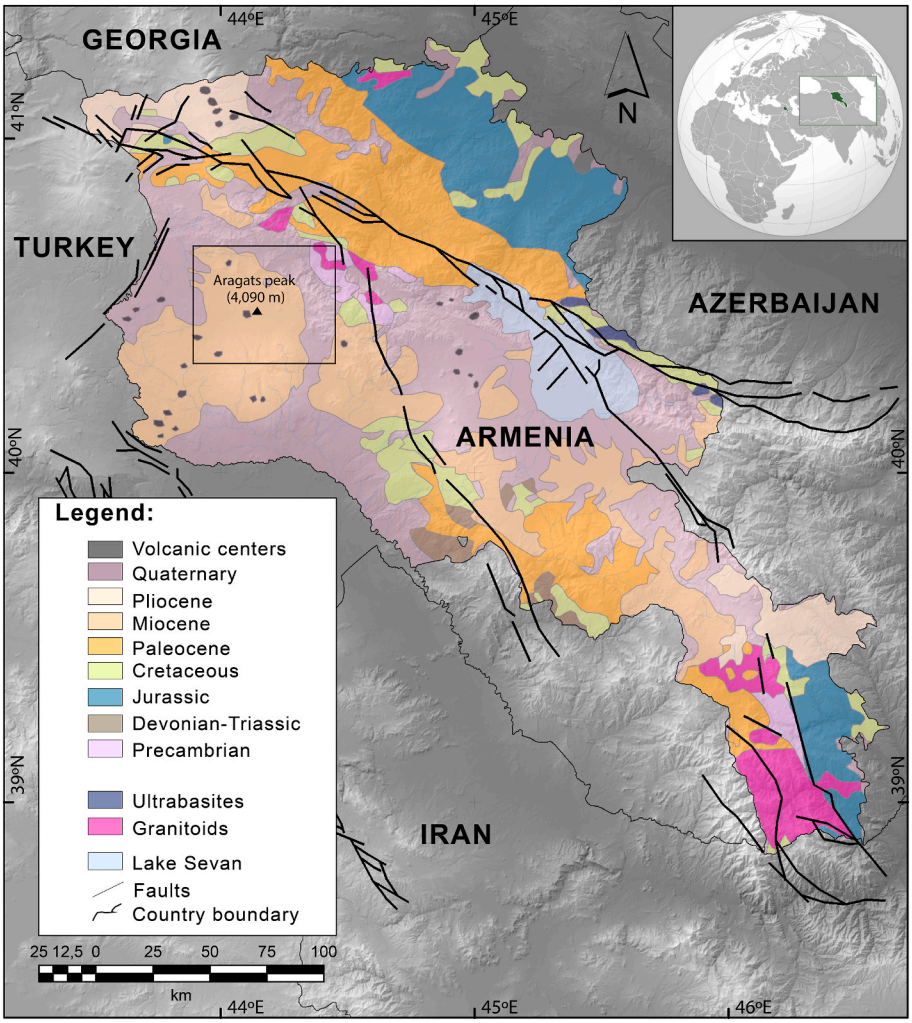

Fig. 1. Geological setting of the study area.

(Հայկական լեռնաշխարհ), within the South-Western Asia (Neill et al., 2013, 2015; Tsereteli et al., 2016; Sherriff et al., 2019, 2021, 2024; Gasparyan and Glauberman, 2022; van Hinsbergen et al., 2024) (Fig. 1). Most of neotectonics activity primarily focus along two major active large-scale faults (Westaway, 1990; Tsereteli et al., 2016; Mergevosovich et al., 2024; Ocakoğlu et al., 2024), the Pambak-Sevan-Syunik Fault (Karakhanyan et al., 2013) and the Garni Fault. These structures exhibit alternating dextral strike-slip motion and components of both reverse and normal faulting, significantly influencing the geological landscape and evolution of recent basins (Ritz et al., 2016; Trifonov et al., 2017; Shalaeva et al., 2023). Notably, these fault systems have been responsible for historical earthquakes with magnitudes exceeding Mw 7 (Karakhanyan and Abgaryan, 2004).

Within this tectonic context, Pliocene-Quaternary volcanism is widespread, spanning a range of volcanic compositions from basalts to rhyolites comprising five volcanic provinces with polygenic and monogenetic volcanic activity (Gevorgyan et al., 2020). Mount Aragats stands out as one of the largest volcanoes of the Armenian Highlands, displaying four distinct polygenic stages from 2.5 Ma to 0.49 Ma (Halama et al., 2020), characterized by varying compositions from trachybasalts to trachydacites (Paffengol'ts and Ter-Mesropyan, 1968).

The Mount Aragats volcanic system hosts numerous vents and cinder cones that form six large ignimbrite units covering an area of 5000 km^2, suggesting important explosive events (Jrbashyan et al., 2012). Age determination based on K/Ar and Ar/Ar data suggests two different ignimbrite sequences spanning from 1.8 to 0.65 Ma. (Gevorgyan et al., 2018). In addition, magmatic intrusions from Lower Paleozoic and Tertiary comprise granitoids together with small-scale gabbroid intrusions, which appear in the north and northeast of the area.

The most recent Quaternary deposits comprise lavas, tuffs and sedimentary rocks comprising alluvial and fluvial conglomerates and lacustrine sediments with palaeontological content. The latter alternates with pyroclastic material from cataclysmic eruptions that interrupted sedimentation (Gevorgyan et al., 2020).

These rocks and sediments are underlying to the north by Jurassic and Cretaceous sedimentary rocks and Proterozoic and lower Paleozoic metasedimentary sequences with different grades and compositions that cover large areas in the northeastern part of the region.

The Mount Aragats slopes exhibit numerous evidence of Pleistocene glacier activity that left their geomorphic and sedimentary imprint in the form of various landform-sedimentary assemblages, such as moraine sets and till deposits. However, before this paper, absolute chronologies were not available for the glaciers of Mount Aragats, but there was a relative time sequence based on the arrangement of the moraines. This sequence was deducted by the comparative analysis of the Last Glacial Cycle in the Alps (Würm glaciation) as a reference model (see Boynagryan, 2020, 2021 and references). This model included the Glacial Maximum, the three Late Glacial stadial and the latest historical advance postglacial. These papers did not specify any location for the Glacial Maximum. However, they did locate the other stages using the alpine chrono-sequence (see Ivy-Ochs, 2015), i.e., the Gschnitz (Oldest Dryas), Daun (Older Dryas) and Egesen (Younger Dryas) stadials and the Fernau (Little Ice Age) historical pulse. Finally, the glaciers reduced to firn basins that disapeared during the second half of the twentieth century (Davoyan, 1971; Tsomaya et al., 1983; Boynagryan, 2020, 2021).

3. Methodology

3.1. Geomorphology and mapping

The mapped area covers a total of ~ 1789 km^2. First, we reviewed the geomorphological features documented in prior studies (Davoyan, 1971; Tsomaya et al., 1983; Boynagryan, 2020, 2021). Subsequently, we generate a geomorphological inventory with new field observations and interpretations from satellite imagery. The glacial and associated landforms map of Aragats mountain was obtained using the most standardized procedure, based on photointerpretation of panchromatic stereo-photos and field observations (Benn and Ballantyne, 2005; Evans, 2012; Seijmonsbergen, 2013; Smith et al., 2006; Chandler et al., 2018). The presented map was designed using the classical legend for geomorphological maps (landform/deposit-process-age represented by symbols and color patterns; Demek, 1972), and the most standardized symbols and nomenclatures for the glacial and glaci-volcanic morphological features (FGDC, 2006; Alcalá-Reygosa et al., 2016; Azzoni et al., 2017; Carrasco et al., 2020, 2023; Pedersen et al., 2020; Soteres et al., 2020; Leontaritis, 2020; Rudolph et al., 2021; Tielidze et al., 2023). A preliminary map included the principal sedimentary formations as moraines (e.g., borders and ridges), alluvial fans, rock glaciers and paraglacial debris slopes. The moraines ridges were digitized as lines and the rest as polygons using topographical breaks visible on the hill-shade/slope models. The location and typology of the former glaciers were also mapped, which have implications for landscape development in the Armenian Highlands.

The map was performed by using ArcGIS 10.8 and QGIS 3.34 software, 3D anaglyph and high-resolution images of Google Earth (2016 Cnes/SPOT, ~15 m spatial resolution), ESRI Imagery (Imagery, 2017, TerraColor, ~15 m spatial resolution and SPOT, ~2.5 m spatial resolution), Bing (BI, 2024, Maxar, ~5 m spatial resolution) and Yandex. The identification of different geomorphological units was supported by previously employed image enhancement, that has been widely used in various fields of research to enhance micro-reliefs not directly observable from digital terrain models (DTM) derived from the processing of LiDAR and drone point clouds. In this regard, the implementation of different tools widely used in archaeology (Štular et al., 2012; Kokalj et al., 2013; Fernández-Lozano and Gutiérrez-Alonso, 2016; Whalley, 2024) have been recently applied to the mapping of glacial geomorphology (Carrasco et al., 2020). In this work, multi-shading techniques were used to distinguish between icecap and icefield plateau glaciers. Furthermore, the Openness algorithm was utilized, which, unlike other shading methods, is free from directional biases, and the reliefs emphasized by Openness do not exhibit horizontal displacements (Yokoyama et al., 2002; Doneus, 2013). Openness allows for detailed determination and mapping of cirque morphology and serves to support the distinction between icecap and icefield areas. Moreover, the Slope gradient has also been implemented as the first derivative of the DTM to highlight the morphology of valleys and moraine crests and to determine hummocks. Finally, the Sky View Factor, utilizing the algorithms developed by Zakšek et al. (2011), was examined to complete the mapping of cirques and to distinguish lava flows from hummocks. This was achieved by identifying shaded regions to highlight linear features that run parallel to the direction of the light source.

Field campaigns during the 2023 and 2024 summer months were conducted to identify features not easily observed from remote sensing data. In these works, direct field measurements were carried out using a handheld GPS, along with photography. The recorded data are: topographic location and relations of landforms and/or geometry, approximate size, shape, orientation, morpho-stratigraphic succession and lithology of moraines and associate's formations. According to Chandler et al. (2018) recommendations, we carry out specific observations to confirm the previous interpretations of process-form relations. Finally, the field works included the sampling for future chronological studies by Cosmic Ray Exposure Dating (CRE).

A critical task in both the desk and fieldwork was to establish the morphostratigraphic succession of the glacial and associated deposits. To this end, and following the most standardized methodologies (Frye and Willman, 1962; Lukas, 2006; Hughes, 2010; Pedraza et al., 2013; Leontaritis, 2020), the positional relationships of the main morainic formations were determined, as a previous step to establish the evolutionary sequence of the Aragats paleoglaciers in their regional context (Carrasco et al., 2015).

3.2. Cosmic ray exposure dating

3.2.1. Sampling

The sampling strategy was based on four fundamental premises: 1) maximizing available resources, 2) collected samples must follow the morphostratigraphic succession of local glacial landforms, 3) bracketing the timing of deposition of the outermost and the innermost moraine formations, and 4) decipher the chronology of intermediate glacial evolutionary stages (Carrasco et al., 2013, 2023). Therefore, the sampling priority was given to the outermost erratic boulders (local Maximum Ice Extent indicators) and those located on moraines crests (stage transit indicators). In this study, 13 samples were collected for numerical exposure dating using ^{36}Cl-CRE from volcanic boulders on the moraines of the Mount Aragats paleoglaciers.

Large stable boulders (>1 m^3) on top of the crest from each moraine, interpreted as the geomorphic marker of the onset of ice withdrawal, were sampled to avoid till-shielded surfaces and to minimize the effect of potential post-glacial boulder rotation: Boulders located in areas affected by peri- and paraglacial processes were also dismissed (Dortch et al., 2013; Carrasco et al., 2015) (Figs. 2 and 3). Samples from flat surfaces and away from highly weathered areas, edges, joints, and cracks were taken (Akçar et al., 2011; Stroeven et al., 2011). The samples were collected using a chisel and a hammer from the upper surface of the boulders to a depth of up to 4–5 cm. Sampling locations were recorded with a hand-held GPS, and the dip/orientation of the sampling surface and the topographic shielding were measured with a clinometer and a compass. All samples correspond to moraine boulders of volcanic lithologies.

3.2.2. Sample preparation for chlorine 36 measurements

In this studied volcanic lithologies and following Schimmelpfennig et al. (2009, 2011), a "whole rock" approach has been used to determine the exposure ages from in situ produced ^{36}Cl due to the lack of Ca- and K-rich phenocrysts with low (i.e., ≤20 ppm) natural Cl content (to minimize the ^{35}Cl production pathway).

First, samples were crushed and sieved to obtain a 250–1000 μm fraction. This material was leached for 3 h in ultra-pure water and then dried. Subsequently, after 1 day on a shaking machine in a solution of HNO3/HF acids (both supra pure; 0.08 ml HNO3 (65 %) and 0.36 HF (40 %) per g sample), ~20 % of the total mass was dissolved. After being dried, 2g of samples were collected for total elemental composition determination, as ^{36}Cl has many production pathways. To be able to determine both ^{35}Cl and ^{36}Cl concentrations, all samples were spiked with a chlorine carrier (6 mg of Cl per g of the carrier whose ^{35}Cl/^{37}Cl is 300). The material was then dissolved in HF (supra pure, 40 %, 4.5 ml per g sample). After 2 days on a shaker table, the samples were centrifuged in 250 ml falcon tubes to separate the solution from the gel formed during dissolution.

$AgNO_3$ was added to the solution to precipitate AgCl (two days in dark conditions). AgCl was recovered and cleaned several times with ultra-pure water, then dried and kept in a dark condition prior AMS measurement. For AMS measurements, the AgCl was transferred and pressed into a nickel cathode. One full-chemistry blank went together with the samples.

The ^{36}Cl and Cl concentrations were measured by isotope dilution by Accelerator Mass Spectrometry at the French AMS national facility ASTER (CEREGE, Aix-en-Provence), and were both normalized to a^{36}Cl standard (SM-CL12 prepared by S. Merchel with a given ^{36}Cl/^{35}Cl-value of (1.428 ± 0.02) × 10–12 (Merchel et al., 2011).

The decay constant of 2.303 ± 0.016 10-6 yr^{-1} used corresponds to a^{36}Cl half-life (T1/2) of 3.014 × 105 years. Analytical uncertainties include counting statistics, machine stability and blank correction (^{36}Cl/^{35}Cl blank ratio is 1.246 × 10–15 ± 25 %). The blank correction represents 0.01–0.11 % of the sample concentrations. All data used to determine ^{36}Cl concentrations are presented in Table 1.

The elemental compositions of the samples to determine the production pathways of ^{36}Cl are presented in Table 2. Due to tight time constrains the elemental composition was done by ICP-OES (ICAP 6500 from Thermo) using four standards (a Merck Certipur multi multi-elements in Suprapur HNO3 6 %, batch n° HC16755392, a Perkin Elmer-TRUQms for titanium (CL13-85TiY-1), a Chemlab uranium standard (CL01 2101.0100; 1000 ppm in 2–5 % HNO3) and. a Chemlab thorium standard (CL01 2041.0100; 1000 ppm in 10 % HNO3)

Fig. 2. Some sampled comprising volcanic disperse erratic boulder from the external areas of the valleys (Marginal Deposits formation, MD). Which provided data for detection of the glacial cycles and the maximum extensions of the ice in each period. The samples are in the plaeoglaciers of: (A) Arkhashan, (B) Artikjur, (C) Gegharot and (D) Getadzor.

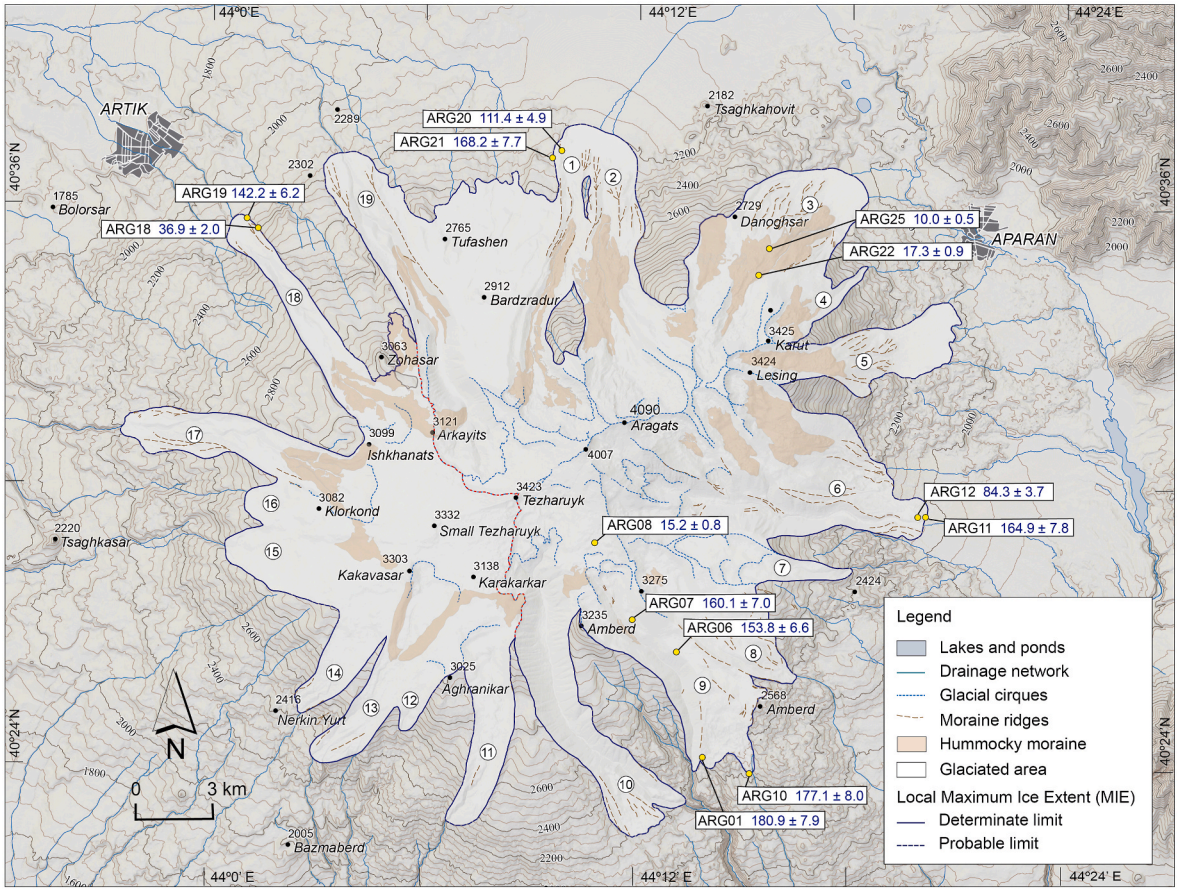

Fig. 3. Cartography of the absolute Maximum Ice Extent of glaciers in Mount Aragats (Aragats Glacial Maximum, AGM). The boxed references indicate the position of the samples used in this work for CRE-dating (Table 4). The numbers in a circle, from 1 to 19, correspond to glacial valleys (Table 5). The red dashed line indicates the boundary between the two types of former glacial systems, ice cap and ice field. (For interpretation of the references to color in this figure legend, the reader is referred to the Web version of this article.)

Table 1
Chemistry information, AMS ratios and ^{36}Cl concentrations.

Sample	Mass dissolved	Spike added	Cl36/Cl35	Uncertainty ^{36}Cl/^{35}Cl (%)	^{35}Cl/^{37}Cl	Incertitude ^{35}Cl/^{37}Cl (%)	AMS cathode	^{36}Cl	±	^{35}Cl	±
	g	at Cl						at/g	at/g	ppm	ppm
ARG01	33.30	3.496E+19	3.16926E-12	3.9867	4.256	1.8027	CQVU	12 364 838	541 005	221.49	15.94
ARG06	30.85	3.4877E+19	3.85561E-12	3.9437	4.706	1.7645	CQVV	12 809 672	553 435	170.21	9.81
ARG07	35.29	3.497E+19	3.48564E-12	4.0392	3.747	1.6978	CQVW	20 595 092	902 372	382.01	40.27
ARG08	36.49	3.4825E+19	6.26556E-13	5.0458	3.774	1.8528	CQVX	3 437 507	184 774	352.22	39.00
ARG10	36.47	3.5001E+19	3.15797E-12	4.2071	3.894	1.6695	CQVY	15 167 042	686 501	298.53	26.27
ARG11	33.95	3.4929E+19	2.08314E-12	4.3867	4.026	1.8297	CQVZ	9 460 438	449 650	272.87	23.28
ARG12	28.52	3.4908E+19	3.10954E-12	3.9715	14.450	1.8047	CQWA	4 787 638	208 854	24.44	0.83
ARG18	26.13	3.4887E+19	9.99435E-13	5.0545	29.800	2.0607	CQWB	1 467 799	80 119	10.41	0.38
ARG19	31.67	3.5022E+19	3.18356E-12	4.0314	14.742	1.6779	CQWC	4 404 386	192 323	21.50	0.70
ARG20	29.94	3.498E+19	2.38090E-12	4.0697	15.634	1.6916	CQWD	3 426 944	151 035	20.99	0.68
ARG21	36.11	3.4877E+19	2.52999E-12	4.2638	3.862	1.7257	CQWE	12 665 525	582 589	313.86	29.44
ARG22	36.89	3.4908E+19	5.18935E-13	4.8371	3.798	1.6650	CQWF	2 739 991	140 168	336.86	32.76
ARG25	33.40	3.4815E+19	3.45063E-13	4.8845	3.927	1.7958	CQWG	1 739 195	90 510	310.92	28.40
Blank		3.51043E+19	1.77131E-15	25.1757	205.115	1.8161	CQWH				

3.2.3. Age determination

The final age calculation followed the approach by Schimmelpfennig et al. (2009), allowing the determination of ^{36}Cl production rates presented in Table 3. The original Excel sheet of Schimmelpfennig et al. (2009) was modified, and sea level high latitude spallation production rates were updated as follows: 42.2 ± 4.8 at/g Ca (Schimmelpfennig et al., 2011); 148.1 ± 7.8 at/g K (Schimmelpfennig et al., 2014); 13 ± 3 at/g Ti (Fink et al., 2000) and 1.9 ± 0.2 at/g Fe (Stone et al., 2005). For the production rate of epithermal neutrons from fast neutrons in the atmosphere at the land/atm interface, the value of 696 ± 185 from Marrero et al. (2016) was used. All productions were scaled following Stone (2000) polynomial.

To consider the ^{36}Cl production from radiogenic elements, a mean lava flow age of 500 ka was used for all samples. Exposure ages without denudation are presented in Table 4 as well as maximum denudation rates considering the lava flow age as a maximum age. As radiogenic production may not be well constrained, some authors reported negative ages when radiogenic production was accounted for (Athanassas et al.,

Table 2
Composition used to determine the ^{36}Cl production.

Sample	CaO	K_2O	TiO_2	Fe_2O_3	SiO_2	Na_2O	MgO	Al_2O_3	MnO	P_2O_5	H_2O	Li	B	Th	U
	[wt.%]	[wt.%]	[wt.%]	[wt.%]	[wt.%]	[wt.%]	[wt.%]	[wt.%]	[wt.%]	[wt.%]	[wt.%]	[ppm]	[ppm]	[ppm]	[ppm]
ARG01	7.44	5.23	1.70	3.38	66.10	6.69	0.17	9.13	0.11	0.02	0.04	5.92	44.76	60.29	9.87
ARG06	6.17	4.71	1.83	3.66	69.24	6.45	0.26	7.53	0.11	0.01	0.03	8.98	56.34	36.00	10.77
ARG07	4.26	4.97	1.75	6.82	56.36	4.62	6.39	14.62	0.16	0.01	0.04	14.23	43.41	84.87	8.50
ARG08	5.90	6.85	2.30	8.60	53.93	6.91	3.95	11.31	0.19	0.02	0.04	7.28	44.38	103.31	10.77
ARG10	7.86	5.89	2.47	3.79	66.42	3.32	0.32	9.26	0.15	0.42	0.08	6.52	39.87	97.43	10.18
ARG11	3.45	3.23	1.54	5.71	67.50	5.38	4.94	8.08	0.13	0.02	0.02	10.06	48.89	133.96	13.90
ARG12	7.29	7.35	2.04	4.50	64.79	3.24	0.37	9.81	0.13	0.40	0.08	6.91	53.17	122.63	12.68
ARG18	4.38	4.51	2.11	7.62	58.31	2.61	4.41	15.82	0.18	0.02	0.04	12.48	33.41	93.22	9.37
ARG19	1.11	4.59	2.59	6.15	67.27	2.22	0.41	15.47	0.13	0.00	0.04	10.01	35.08	83.68	7.76
ARG20	7.35	2.18	2.42	7.43	59.43	3.25	7.77	9.94	0.17	0.03	0.02	4.21	64.23	140.83	15.09
ARG21	5.69	3.26	2.29	6.10	66.22	5.79	0.02	4.55	0.24	0.00	0.04	5.42	45.08	104.81	11.01
ARG22	2.73	3.47	2.38	4.94	63.13	7.74	2.26	5.24	0.29	0.00	0.07	8.45	48.24	99.56	10.24
ARG25	3.52	3.20	1.84	7.40	61.26	5.23	4.76	7.36	0.12	0.04	0.03	6.33	49.42	123.55	13.18

Table 3
^{36}Cl production rates in the studied samples. The following, sea level high latitude spallation production rates were used: 42.2 ± 4.8 at/g Ca (Schimmelpfennig et al., 2011); 148.1 ± 7.8 at/g K (Schimmelpfennig et al., 2014); 13 ± 3 at/g Ti (Fink et al., 2000) and 1.9 ± 0.2 at/g Fe (Stone et al., 2005). For the production rate of epithermal neutrons from fast neutrons in atmosphere at land/atm interface the value of 696 ± 185 from Marrero et al. (2016) was used. All productions were scaled following Stone (2000) polynomial.

Sample	$P_{spallation}$	$P_{epithermal}$	$P_{thermal}$	P_{muons}	$P_{radiogenic}$	P_{total}
	[at^{36}Cl g^{-1} a^{-1}]					
ARG01	46.64	11.90	21.95	1.51	0.82	82.83
ARG06	60.00	13.04	23.39	1.60	0.44	98.47
ARG07	61.34	30.94	56.31	1.36	1.85	151.80
ARG08	102.84	34.25	54.22	2.11	1.87	195.29
ARG10	53.65	16.38	30.29	1.67	1.18	103.18
ARG11	25.01	13.27	25.55	0.75	2.07	66.64
ARG12	56.94	1.23	2.22	1.67	0.12	62.18
ARG18	38.40	0.57	1.07	1.05	0.05	41.15
ARG19	32.20	1.12	2.18	0.62	0.08	36.21
ARG20	29.71	1.22	2.26	1.24	0.15	34.57
ARG21	34.60	18.76	33.17	1.14	1.56	89.22
ARG22	45.36	29.13	51.79	0.94	1.99	129.22
ARG25	42.02	25.63	45.49	1.01	2.07	116.22

2016; Charton, 2024). Ages and maximum denudation rate (infinite times) without the radiogenic contribution (lava flow age set to zero) are also presented in Table 4.

However, despite some samples with high ^{35}Cl content, radiogenic production did not sufficiently influence so much the exposure ages.

4. Results

4.1. Glacial geomorphology

During the Maximum Ice Extent (MIE) in the Mounts Aragats area, marked by the outermost moraine ridges, 19 glaciers have been identified with a total length (tongue and cirque) of up to ~17 km, characterized by tongues with ice thicknesses of up to ~350 m and some glaciers that descended from about 3900 m asl to 2040 m asl (Fig. 3, Table 5).

4.1.1. Glacial cirques morphology

Glacial cirque (hereafter cirque) is a term that originally referred to specific landforms due to glacial erosion and is characterized as a truncated elliptical paraboloid (Charpentier, 1823). At present, cirques are defined as armchair-shaped hollows exhibiting steep headwalls and relatively deep and flat floors, originating by glacial overdeepening (Gordon, 1977; Evans and Cox, 1974; Benn y Evans, 2010; Barr and Spagnolo, 2015). Prior studies have demonstrated that cirque morphometric attributes are suitable indicators of paleoclimate conditions (Evans, 1977; Olyphant, 1977; Graf, 1976; Peterson, 1968; Mitchell, 1996). Therefore, cirque landforms are useful as paleoclimatic indicators (Peterson, 1968; Graf, 1976; Barr and Spagnolo, 2015).

In the Aragats area, 18 cirques were mapped, most of which tend towards isometry and are simple and unitary, although there are also compound and staircase cirques (Fig. 4, Table 6). They show limited vertical incision capacity, considerable variation in size, and are predominantly oriented towards the NW and the SE (Fig. 5). The larger and intermediate cirques are located on the main divides of higher

Table 4
^{36}Cl exposure ages (no denudation) and maximum denudation rates considering a mean lava flow age of 500 ka. Exposures ages and maximum denudation rates (infinite time) are also presented without the radiogenic correction (lava flow age set to zero). The morphostratigraphic formations correspond to those defined in this work.

Samples	Morphostratigraphic formations	Lava flow age = 500ka		Lava flow age set to 0		^{35}Cl ppm
		Age (no denudation) (ka)	Max denudation m/Ma	Age (no denudation) (ka)	Max denudation m/Ma	
ARG01	Marginal Deposits (MD)	180.9 ± 7.9	4.9 ± 0.2	185.5 ± 8.1	5.0 ± 0.2	221.49
ARG06		153.8 ± 6.6	5.5 ± 0.2	155.6 ± 6.7	5.6 ± 0.2	170.21
ARG07		160.1 ± 7.0	6.5 ± 0.3	165.5 ± 7.3	6.4 ± 0.3	382.01
ARG08	Hummocky Moraine (HM)	15.2 ± 0.8	71.9 ± 3.9	18.2 ± 1.0	59.7 ± 3.2	352.22
ARG10	Marginal Deposits (MD)	177.1 ± 8.0	5.2 ± 0.2	182.3 ± 8.3	5.3 ± 0.2	298.53
ARG11		164.9 ± 7.8	6.6 ± 0.3	179.1 ± 8.5	6.3 ± 0.3	272.87
ARG12		84.3 ± 3.7	8.0 ± 0.4	85.0 ± 3.7	8.1 ± 0.4	24.44
ARG18	Border Moraine (BM)	36.9 ± 2.0	19.8 ± 1.1	37.3 ± 2.0	19.8 ± 1.1	10.41
ARG19	Marginal Deposits (MD)	142.2 ± 6.2	4.4 ± 0.2	143.1 ± 6.3	4.5 ± 0.2	21.50
ARG20		111.4 ± 4.9	6.2 ± 0.3	113.1 ± 5.0	6.3 ± 0.3	20.99
ARG21		168.2 ± 7.7	6.2 ± 0.3	176.0 ± 8.1	6.2 ± 0.3	313.86
ARG22	Hummocky Moraine (HM)	17.3 ± 0.9	73.1 ± 3.7	22.1 ± 1.1	56.5 ± 2.9	336.86
ARG25		10.0 ± 0.5	129.4 ± 6.7	15.5 ± 0.8	82.2 ± 4.3	310.92

Table 5
Morphometric parameters of paleoglaciers in the Mount Aragats.

Nº	Paleoglacier		Length (m)	Length 3D (m)	Terminus (m asl)	Summit (m asl)	Area		Max ice thickness (m)
							km	%	
1	Getadzor	Գետաձոր	14100	14330	2183	3816	22.6	5.0	180
2	Rapi	Ռապի	12437	12584	2188	3546	32.2	7.2	90
3	Nigavan	Նիգավան	10510	10676	2032	3501	34.3	7.6	80
4	Nigasar	Նիգասար	4966	5125	2258	3367	4.6	1.0	70
5	Aragats	Արագած	9516	9689	2039	3487	15.8	3.5	190
6	Gegharot	Գեղարոտ	14406	14652	2038	3792	60.9	13.5	260
7	Kertutegh	Կերտուտեղ	7649	7723	2362	3212	7.6	1.7	80
8	Shahverd	Շահվերդ	8891	8977	2351	3325	17.2	3.8	160
9	Arkhashan	Արխաշան	13645	13831	2145	3866	27.6	6.1	250
10	Amberd	Ամբերդ	17546	17759	2040	3762	41.9	9.3	360
11	Lernarot	Լեռնարոտ	13233	13372	2186	3373	15.3	3.4	80
12	Agravakar	Ագռավաքար	9486	9541	2585	3376	3.7	0.8	26
13	Aghranikar	Աղրանիքար	11244	11323	2305	3326	20.2	4.5	70
14	Kakavasar	Կաքավասար	9131	9208	2416	3297	10.9	2.4	50
15	Selav-Mastara	Սելավ Մաստարա	8075	8116	2575	3278	16.9	3.8	50
16	Garnhovit	Գառնհովիտ	6791	6829	2743	3261	5.2	1.1	45
17	Metsdzorijur	Մեծձորիջուր	14474	14573	2185	3380	24.2	5.4	110
18	Artikjur	Արթիկջուր	15379	15479	2081	3371	22.4	5.0	80
19	Mantash	Մանթաշ	17268	17504	2111	3917	39.3	8.7	335
*	Area associated with Mantash glacier		9134	9210	2327	3305	27.3	6.1	29

topographic elevations around Aragats Peak, which is the apex of the ancient stratovolcano. The cirques of smaller dimensions are located at the western and eastern ends of the mountain massif, far from the apical zone of Aragats Peak, at lower altitudes (Figs. 3 and 4). According to their plan geometry (Evans and Cox, 1974; Barr and Spagnolo, 2015), the semicircular types (concave cirques), those with elongated basins (oval cirques) and those with a U-shaped morphology (trough cirques) have been identified.

The U-shaped cirques (trough) are mainly located at the western and eastern ends of Mount Aragats. Those on the west sector (Gmbert-Kakavakar plateau) are small hollows excavated into a topographic plateau and coinciding with the area of initiation of the former outlet-type tongues flowing from the summit. Those in the eastern sector (Aragats Peaks) have originated in the marginal domain of the summit divide by the erosive processes characteristic of cirque-type glacial accumulation basins. All of them are simple cirques of smaller

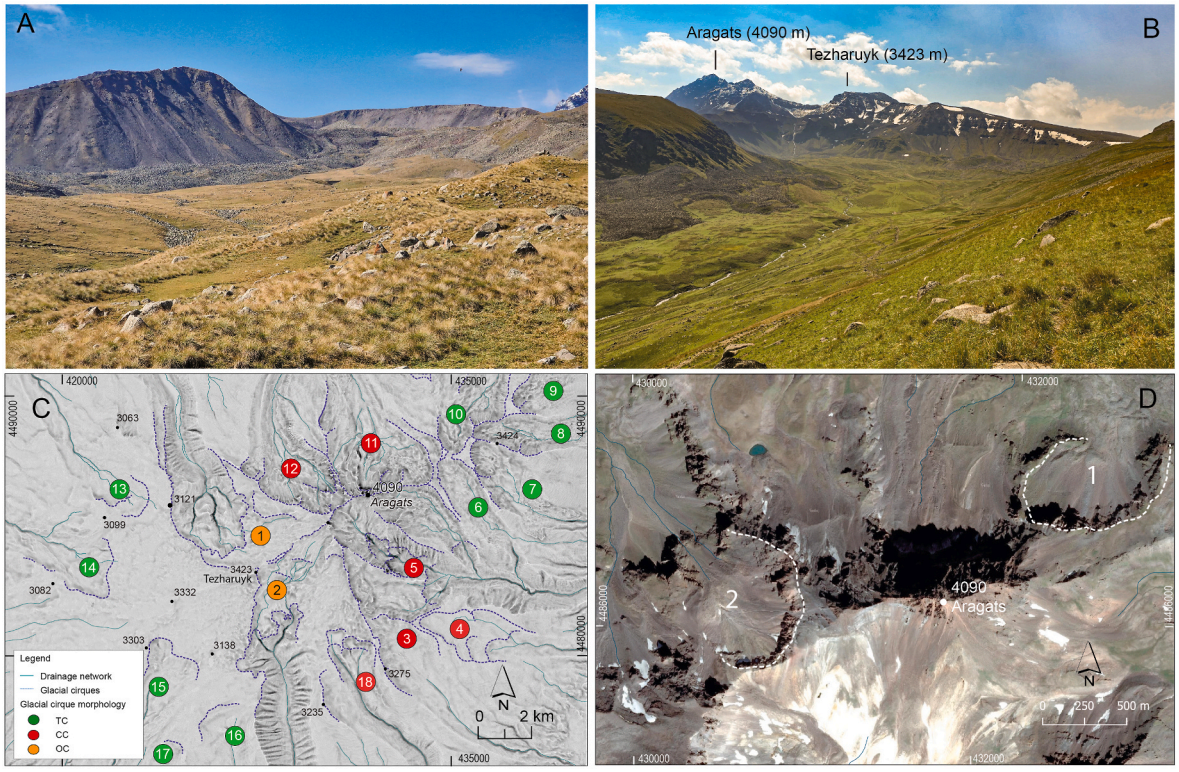

Fig. 4. A) Glacial cirque of Nigavan (background of the image). Several morainic ridges appear at the bottom of the valley (foreground of the image) and the rock glacier tongue (middle ground of the image). B) Glacial cirque of Rapi composed by several compartments and staggered minor cirques (background of the image). On the slopes can see the development of rock glaciers and debris cones. The bottom of the valley is fully occupied by hummocky type supraglacial ablation moraine (middle ground of the image). C) Mapping of glacial cirques carried out based on the Openness algorithm for image enhancement (Table 6). D) Example of minor cirques (1 and 2) controlled by the preglacial volcanic morphology (Yandex image using QGIS34).

Table 6
Basic morphometric parameters of glacial cirques of Mount Aragats (extracted with ACME GIS tool; Spagnolo et al., 2017).

Nº	Emin	Emax	H	Emean	Slope mean	Aspect mean	Type	Description
1	2635	3613	978	3113	16	298	OC	Complex elongated cirque, staircased. Connected to other cirques. With secondary minor cirques.
2	2659	3509	850	3121	17	176	OC	Complex elongated cirque, staircased. Connected to other cirques. With secondary minor cirques. With a disfluency that generates two emissary tongues.
3	2905	3419	514	3102	12	137	CC	Minor concave cirque. Connected to other cirques.
4	2792	3206	414	3009	8	85	CC	Simple concave cirque, slightly staircased.
5	2830	4090	1260	3357	23	118	CC	Complex concave cirque with three compartments, two concaves and another elongated, staircased and with notable overdeepened. Connected to other cirques and with secondary minor cirques.
6	3125	3540	415	3305	14	144	TC	Trough cirque, very slightly overdeepened. Connected to other cirques.
7	3017	3588	571	3221	16	134	TC	Complex trough cirque with several minor compartments. Very slightly overdeepened and connected to other cirques.
8	2995	3576	581	3222	21	87	TC	Simple trough cirque. Very slightly overdeepened and connected to other cirques.
9	3046	3400	354	3172	18	53	TC	Simple trough cirque. Very slightly overdeepened and connected to other cirques.
10	2880	3555	675	3154	16	16	TC	Complex trough cirque with two compartments. Very slightly overdeepened and connected to other cirques.
11	2962	4087	1125	3271	18	352	CC	Complex concave cirque with several minor compartments. Connected to other cirques.
12	2871	3992	1121	3237	21	333	CC	Complex concave cirque with several minor compartments. Connected to other cirques.
13	2925	3068	143	2991	6	329	TC	Simple trough cirque. The plateau U-shaped cirque.
14	2910	3141	231	3023	9	316	TC	Simple trough cirque. The plateau U-shaped cirque.
15	2971	3257	286	3089	8	219	TC	Simple trough cirque. The plateau U-shaped cirque.
16	2858	3090	232	2980	9	163	TC	Simple trough cirque. The plateau U-shaped cirque.
17	2909	3000	91	2954	8	204	TC	Simple trough cirque. The plateau U-shaped cirque.
18	2780	3263	483	3052	15	137	CC	Complex concave cirque, staircased. Connected to other cirques. With secondary minor cirques.

Legend: Emax (m asl), maximum elevation (altitude) of cirque headwall. Emin (m asl), minimum elevation (altitude) of cirque floor. H (m asl), difference between minimum elevation of cirque floor. Emean (m asl), value of mean contour line of cirque elevations. Slope mean (degrees), mean slope value for the delimited cirque area. Aspect mean (degrees north), mean aspect value in degrees north (0–360° interval). OC, elongated cirque. CC, concave cirque. TC, trough cirque.

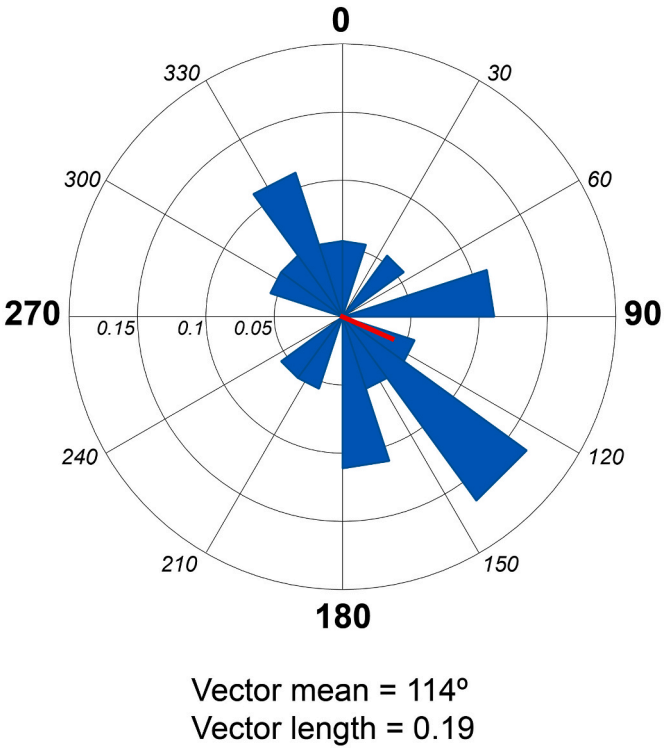

Fig. 5. Distribution of glacial cirques according to aspect.

dimensions (between 0.5 and 9.6 km^2 area 2D).

The semicircular cirques (concaves) are in the central area of Mount Aragats and are hosted in the ridges, peaks, and edges forming the highest elevations of these mountains. Some of these cirques have complex morphologies with minor cirques embedded in the main ones, stepped cirques, and armchair cirques forming saddles that interconnect different valleys. In general, they are large in area (between 5.2 and 18.4 km2 area 2D) and have notable cliffs on their headwalls (H up to c. 1200 m).

Finally, the elongated cirques (oval) are the headwaters of two large valleys that form an NNW-SSE morphostructural corridor. Both valleys are interconnected at the head and built in the eastern limit of the topographic plateau. The oval cirques of this area have a planoconcave morphology, with a series of secondary minor staircase cirques. They present large dimensions at the head (between 8.9 and 14.6 km^2 area 2D), forming a small topographic plateau. Due to this type of morphology, these cirques can be interpreted as an intermediate case between the U-shaped and the semicircular types.

In the Aragats area, the maximum elevation (Emax) of the cirques coincides with the main divide of the stratovolcano. Although some cirques on opposing slopes are interconnected, it has not been possible to identify any cirque truncation (White, 1970) related to a buzzsaw-type relief evolution process, as proposed in other mountain areas of the world (Mitchell and Montgomery, 2006; Foster et al., 2008).

According to the available data, the cirques of Mount Aragats are comparable to those of other mountains in the regional context, regarding those analyzed in the Southwestern Anatolia (Çılğın and Bayrakdar, 2018, 2020; Evans et al., 2021; Çilğın et al., 2024). These cirques show similar or larger dimensions but are more complex, better defined, and mainly exhibit northern aspects. However, they are convergent in morphology and orientation with those described in the Eastern Black Sea Mountains (Şimşek et al., 2023).

4.1.2. *Glacial valleys and deposits*

The ice masses that started in the central sector of the Aragats Peak, both to the north and south, caused deep vertical incisions in the terrain, giving place to large glacier valleys with long-distance tongues and notable moraine complexes. However, the emissaries that started from the marginal areas of the Aragats Peak to the east and from the topographic plateau located to the west developed valleys with little vertical incision and smaller ice tongues forming intermediate glacier valleys. In both cases, some of these tongues crossed steep slopes, forming a kind of slope glacier.

Most of these valleys have a well-developed U-shaped morphology and sometimes present shoulder pads of embedding sequences (Fig. 6). The larger lateral moraines generally start attached to the slopes and evolve into border moraines that define the limit of the old glacial

valley. Their morphology is perceptible in the landscape, and their ridges are very sharp. However, in some cases (for example, the Amberd glacier, 10 in Table 5), they have suffered postglacial erosion processes, such as debris flows. In all cases where the tongues flowed embedded in valleys with extra-glacial rock walls, there are many debris due to paraglacial processes, including debris flow, debris slides, rock glaciers or protalus rampart (Fig. 6C).

Considering the outermost moraines formations reflecting the local maximum ice extent (MIE), the large valley glaciers had lengths between <18 km and >10 km, depths of ~300 m; the glacial terminus was between ~2188 m and ~2040 m and overcoming unevenness of ~1800 m or ~1000 m depending on the case (Table 5). The most prominent valleys are located around Aragats Peak, forming the central sector of the Mount Aragats area. The Getadzor and Rapi glacier tongues (1 and 2 in Table 5) converged in the middle section of their course, leading to a single glacier that reached the piedmont plain, giving rise to an elephant's foot termination and a large outwash plain with an alluvial fan system. The tongues of glaciers located to the south (Arkhashan and Amberd, 9 and 10 in Table 5) had a common feeding basin conditioned by the subglacial topography, giving place to a subsequent difluence with two independent tongues. These glaciers and the Mantash glacier (19 in Table 5), located to the north, were connected at the head during the glacial advances.

The intermediate valleys are located to the west in the southern sector of the topographic plateau and the east on the eastern edge of the ridge-type summit. During the MIE, these valleys hosted glaciers ranging in lengths from <10 to >4.8 km, maximum thicknesses of ~190 m, the glacial terminus was between ~2040 m and ~2740 m and overcoming unevenness of ~1450 m or ~500 m depending on the case (Table 5). The Gegharot and Nigavan glacier tongues (6 and 3 in Table 5) resulted from the confluence of several tongues forming an ice mantle convergent with a slope glacier. This glacier expanded into the piedmont, creating an irregular front conditioned by the preglacial morphology of the bed and extensive outwash plains also developed giving rise to a system of alluvial fans. Some glaciers originated in the topographic plateau area, such as the Kakavakar, Selav-Mastara and Garnhovit glaciers (14, 15, 16 in Table 5) showing a continuity between the morphology of former accumulation and discharge zones. However, in other glaciers of this area it is possible to differentiate the morphology of accumulation by a trough-type cirque and that of discharge by a well-developed valley.

The glacial deposits of Mount Aragats are diamictons composed of boulders and cobbles with scant gravel and sand matrix, without apparent internal structures and weakly compacted. In some areas, they contain scattered lenses of laminated sands that correspond to fluvial deposits. All of these are composed of volcanic materials, predominantly andesites and basaltic andesites and dacites, basalts and ignimbrites to a lesser extent. The most significant volume of sediments is located on the slopes of the valleys, forming lateral moraines in which a sequence of deposits comprising from bottom to top, subglacial lodgment till, subglacial melt-out till and supraglacial melt-out till (Fig. 7). The identification of these till types are possible by the variation in fine grain material, degree of compaction and the presence of fluvio-subglacial channels. The deposits located on the valley floor are discontinuous due to some rocky thresholds but include a sequence of vertical accretion of tills like the one described above.

Two types of formations appear above these sequences that were previously described: (1) a system of massive boulders forming minor lateral moraines and arcuate moraines (Fig. 6B) and (2) a system of debris that covers the former glacial bed, presenting numerous flow folds (e.g., grooves and ridges). Because of their position and morphology, the formers are interpreted as recessional moraines that indicate the retreat of the glacier. The latter sometimes fossilize the recessional moraines and are interpreted as hummocky-type ablation moraines corresponding to an evolutionary stage of readvance (Fig. 8). The hummocky deposits are present in almost all the valleys, although they acquire notable dimensions in those associated with the Aragats Peak sector. Compared to the general till, those corresponding to the formations at the bottom of the valley present debris with a greater abundance of large boulders and lithological variety, including pyroclastic rocks and volcanic tuffs (Fig. 7A and B).

4.2. Glacial formations and morphostratigraphic succession

The evolutionary sequence of these glaciers was established using the morphostratigraphic succession of moraines and other associated deposits (mainly peri- and paraglacial debris) as primary indicators. Up to three morainic formations and several associated slope debris were identified in the glacier's basins. According to the most standardized

Fig. 6. A) Gegharot river glacial valley (6 in Table 5) showing the U-shaped morphology and the ridges of border lateral moraine formation (dotted line). B) Rapi glacial valley (2 in Table 5): (BM) the principal lateral moraine or border lateral moraine, (ILM) minor internal lateral moraines, (HAIM) valley floor occupied by the hummocky-type ablation supraglacial moraine. C) Amberd river glacial valley (10 in Table 5): (BM) the principal lateral moraine or border lateral moraine, (BBM) boulders field of the border lateral moraine, (S) solifluction lobes, (Df) debris flow. D) Arkhashan river glacial valley (9 in Table 5); dashed lines mark the ridges of the principal lateral moraine or border lateral moraine (BM), arrows indicate erratic boulders corresponding to marginal deposits formation (MD).

Fig. 7. Glacial deposits (tills) in Mount Aragats. General characteristics: diamicton, bi-modal or poli-modal, pebbles, cobbles, and boulders matrix supported. A) The hummocky-type ablation supraglacial moraine on the glacial terminus of Nigavan former glacier (3 in Table 5). B) supraglacial melt-out till corresponding to the ablation supraglacial moraine described in (A) (massive and poli-modal deposit). C) Glacial deposits on the glacial terminus of Rapi former glacier (2 in Table 5): (1) current soil, (2) supraglacial ablation till (massive and poli-modal, very weakly compacted), (3) subglacial melt-out till (weakly fissile and compacted, bi-modal), the arrow indicates a laminated deposit corresponding to a subglacial fluvial channel, (4) subglacial lodgment till (Highly fissile, compacted diamicton with some bullet-shaped and facetted clasts, (5) current debris.

Fig. 8. Glacial deposits in the Rapi valley (2 in Table 5). (BM) the principal lateral moraine or border lateral moraine formation; (ILM) minor internal lateral moraine of glacial retreat (internal moraines formation); (HAIM) hummocky-type ablation supraglacial moraine (internal moraines formation). The arrow indicates the moraine (ILM) of the former glacial terminus fossilized by the advance of the covered glacier that generated the hummocky formation.

classifications (see, for example, Zasadni, 2007), moraines arrangement is characteristic of a continuous accretion process. However, in some valleys, internal moraines show an overlapping process.

The first and outermost formation is called “marginal deposits” (MD; Fig. 6D) and consists of scattered erratic boulders that appear beyond the domain of the major lateral moraines. These boulders indicate the maximum ice extent (MIE) documented in the Aragats area during the glaciation stages. The most external boulders of this MD formation correspond to the local absolute glacial maximum (Aragats Glacial Maximum; AGM). The second formation comprises the intermediate deposits formed by a set of major lateral moraines. Given its topographic position limiting the valley into which the glacial tongues flowed, this formation was called “border moraine” (BM; Fig. 6). This BM formation marks the boundary between the internal and external domains of the glacial valleys and, therefore, the transition between glaciation stages (expansion-stabilization of the ice) and deglaciation stages (retreat-disappearance of the ice). The dimensions of the BM formation represent a prolonged phase of material accretion and, therefore, a period of maximum stabilization of local glaciers. Due to its excellent preservation and presence in all valleys, this BM is the morphostratigraphic reference to establish the evolutionary sequence of glaciation in this area. The third formation corresponds to the set of innermost deposits within the valley bounded by the BM formation, so the term "internal (I)" has been applied to all of them. This formation is the most complex and consists of several sequences of deposits that indicate the period of generalized retreat or deglaciation and the transit between the glacial and post-

glacial stages.

The initial stages of retreat are indicated by inner lateral moraines of smaller dimensions than the BM formation, although they have similar morphological characteristics and are generally attached to their inner slopes. This formation of minor "internal lateral moraines" (ILM) has a much more irregular distribution and is not always well defined (Fig. 6B). The rest of the glacial formations inside the valleys are deposits located in the former glacial bed and generally correspond to supraglacial tills. The first and most prominent of these supraglacial formations are "hummocky-type ablation internal moraines" (HAIM), which are very well developed in some valleys and characterized by their remarkable thickness and continuity. They are typical ground moraines composed of boulders and large boulders, which are generally irregular and without any classification, with a labyrinthine morphology defined by mounds, arcuate ridges, and hollows (Fig, 6B, 7A, 7B, 8). Their morphological characteristics agree with those described for supraglacial hummocky moraine (Benn and Evans, 2010). The arcuate ridges are the dominant ones in the morphology in the initial portion of the valley, showing clear signs of flow and thrust and some convergence with a rocky glacier. However, the labyrinthine reliefs of mounds and hollows dominate in the lower sector, where the indicators show clear signs of stagnation and ablation. According to these differences, it can be concluded that these hummocky formations show genetic processes following those proposed in two hypotheses under discussion: (1) ablation stagnation (Johnson and Clayton, 2003; Peterson and Johnson, 2018) and (2) the flow-pushing (Hambrey et al., 2011).

In several valleys, it was observed that these HAIM partially fossilize the previous ILM formation and correspond to an evolutionary stage of ice readvance (Fig. 8). This evolutionary sequence explained the genesis of this large ablation moraine in several stages. With the first retreats of the glaciers indicated by the ILM moraines, the dismemberment of plateau glaciers began, significantly increasing the ice-free reliefs. In those ice-free walls, para-periglacial processes cause a large volume of debris slides, which are difficult to evacuate, giving rise to debris-covered glaciers of different dimensions and, finally, to HAIM formation.

The last internal formation identified corresponds to the arcuate "recessional internal moraines" (RIM; Fig. 4A, B, 6B) that appear in the heads of the valleys occupying part of the domain of the former cirques. The persistence of the small residual glaciers is very uneven in each valley; therefore, the formations of the debris falls and slides (talus, cones, fields, etc.), the protalus ramparts, and the rocky glaciers are indicators of the post-glacier stage, also have very uneven development. (Figs. 4A and 6B).

4.3. CRE chronology

The first-order chronology of the glacial fluctuation in the Mount Aragats, aiming to decipher the extent of the MIE, the chronology of intermediate ice oscillations and the onset of local deglaciation, has been established based on 13 ^{36}Cl cosmogenic ages spread across the best-persevered moraine ridges hosted in the massif (Table 4). The following ages are presented, considering no denudation. The most comprehensive chronology comes from the Amberd Valley (9 in Fig. 5) on the southern flank of Mount Aragats. In this site, from the outermost to the innermost moraines, two samples indicate that moraines representing the MIE were deposited at 180.9 ± 7.9 ka (ARG01) and 177.1 ± 8.0 ka (ARG10). Up-valley, three samples collected in stratigraphic order indicate glacier fluctuations culminating at 153.8 ± 6.6 ka (ARG06), 160.1 ± 7.0 ka (ARG07) and 15.2 ± 0.8 ka (ARG08). To the east, one sample from the outermost moraine and another from the immediately inner moraine of lobe six yield ages of 164.9 ± 7.8 ka (ARG11) and 84.3 ± 3.7 ka (ARG12). In the northeastern flank of Mount Aragats, two samples taken from hummocky moraines in the intermediate portion of the Danogshar ice lobe (3 in Fig. 5) yield ages of 17.3 ± 0.9 ka (ARG22) and 10.0 ± 0.5 ka (ARG25). In the northern slope of the study area, two samples from the outermost moraines of the ice lobe 1 give ages of 168.2 ± 7.7 ka (ARG21) and 111.4 ± 4.9 ka (ARG20). Lastly, flowing to the northeast, two samples from the outermost moraine belt of the glacier lobe near Artik provide ages of 142.2 ± 6.2 ka (ARG19) and 36.9 ± 2.0 ka (ARG18).

5. Discussion

5.1. The former Mount Aragats glacial system

According to its evolutionary history, Mount Aragat can be considered a complex stratovolcano, but its topographical structure is that of a small plan-convex asymmetric shield (Chernyshev et al., 2002). The volcanic system has about 52 km maximum length, with the main crater located in the northeastern forming alienations of summits about 4000 m asl, while in the southwest, the topography is defined by plateaus that culminate about 3000 m asl. The morphological control exerted by the reliefs' alignment of the main crater provides Mount Aragats the characteristic morphology described in many other glaciovolcanic edifices (Pedersen et al., 2020), that is, a dome-shaped physiognomy with a system of radial-centrifuges glacial valleys (Fig. 9). The current morphology of the summits of Mount Aragats displays an evident contrast between the western and the central and eastern sectors (Fig. 10). The former sector has a flat-topped topography located between 3000 and 3400 m asl and with shallow hills and valleys that generally end at the edge of the plateau. The central and eastern sectors have sharp-topped topography with peaks and arêtes projecting above the average topography of the plateau. This area reaches the maximum elevations of the region (Aragats Peak, 4090 m asl) with cirques headwalls forming divides of large valleys originating from over-deepening along major fractures. This sector is characterized by a system of coalescent head-basins with a series of valleys radiating from them towards the piedmonts.

Mount Aragats comprised a former glacier system heterogeneously constrained by the local topography. Namely, glaciers in the western sector (Gmbert-Kakavakar plateau) were nearly free of topographic control. In contrast, the ice flow in the central and eastern sectors (Aragats arête) was strongly constrained by the local topography. Given that topographic control is a primary factor for defining a plateau glacier type (Sugden and John, 1976; Benn and Evans, 2010), the morphological characteristics of the Gmbert-Kakavakar plateau were appropriate for the development of an icecap-type, while the Aragats ridges were suitable for the formation of an icefield-type glacier.

The Gmbert-Kakavakar plateau consists of a volcanic highland, primarily composed of basaltic andesites and andesites with remarkable glacial erosion features, such as polished surfaces, striations and roches moutonnee (Fig. 10B). Over this substrate appear numerous disperse erratic boulders and boulder fields formed by peri- and paraglacial processes. Topography forms a uniform slope from ~3000 to 3400 m asl, reaching 3423 m asl at the summit of Tezharuyk. Its morphology has a lobe-shaped irregular contour with a maximum length of ~11.5 km in the NNW-SSE direction and a maximum width of ~8 km in the E-W axis. The general tilting is towards the west and presents an average slope of 3-5°, with minor relief areas up to 7°. In detail, the top of this plateau has an undulating topography due to the presence of linear valleys that formed the headwaters of the outlet-type emissary tongues that originate on this plateau during the glacial stages. In general, these ice tongues formed valley and slope glaciers with lengths ranging between 1.5 and 11 km from the plateau edge to the piedmonts. These geomorphological features are consistent with an icecap-type plateau glacier, which was adapted mainly to the dome shape topography of the pre-glacial relief defined by the volcanic shield.

The summits of Aragats South (3879 m) and Karut (3425 m) are connected through a ridge with NE-SW orientation, forming the typical conical landscape of stratovolcanoes. This area includes the main cone of the Aragats volcanic system, along with smaller ones, which facilitated the development of snow accumulation basins. Here,

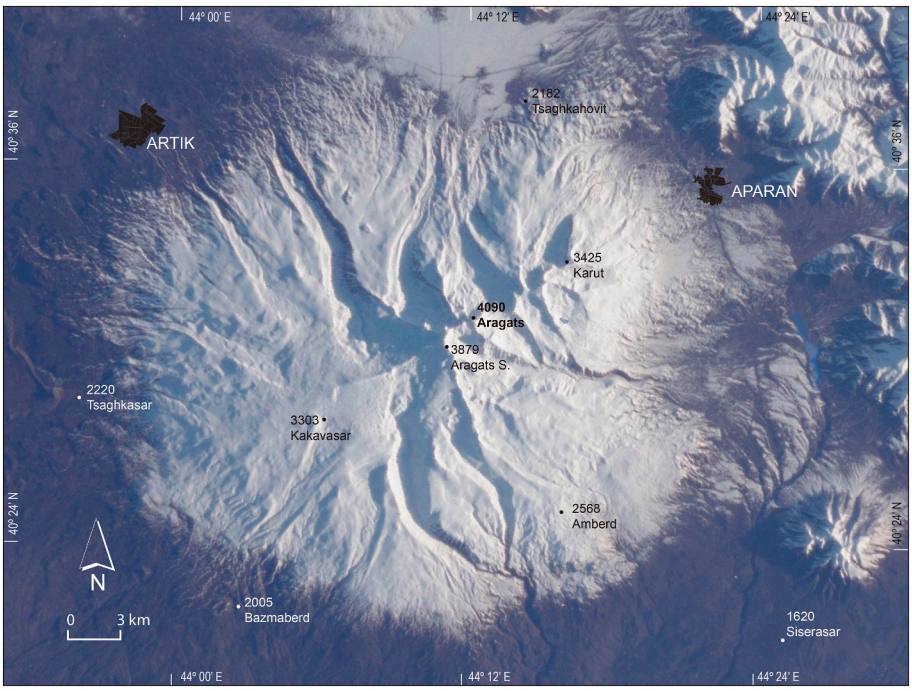

Fig. 9. A modified NASA photograph showing the dome shape of Mount Aragats and its radial valley system (Reference: NASA, 2002, ID STS 059-201-95, Gateway to Astronaut Photography of Earth).

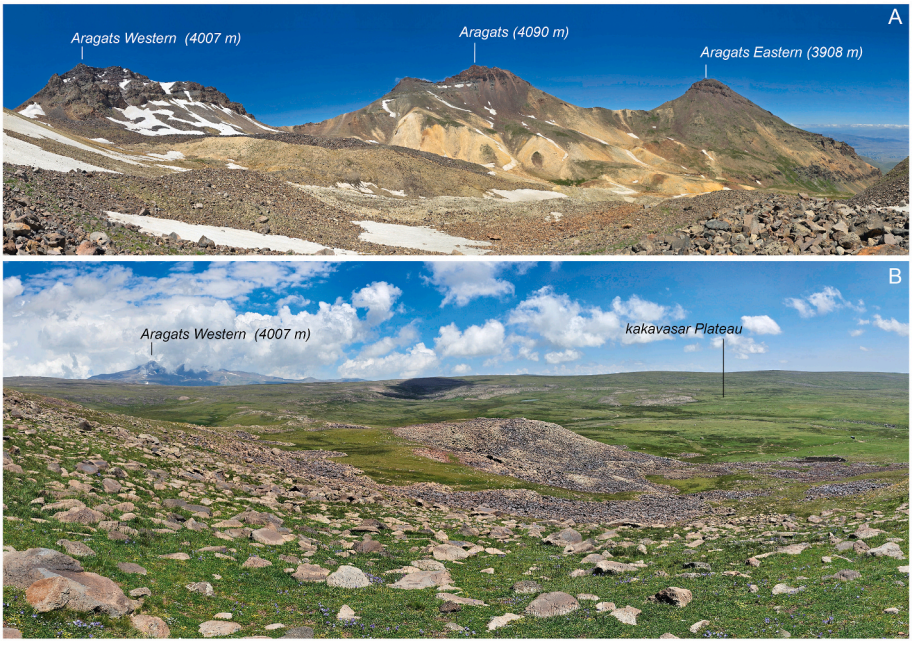

Fig. 10. A) The peaks and ridges system forming the main divide of the central and western sector of Mount Aragats. In the middle ground of the image appears the Aragats Peak (4090 m), the highest summit of these mountains. B) Kakavasar topographic plateau (3150 m average height) in the western sector of Mount Aragats.

morphological evidence indicates the existence of interconnected glacial cirques (Fig. 4C). These landforms are hosted into volcanic materials, rising about 400–700 m above the volcanic plateau, with summits averaging ~3800 m reaching a maximum altitude of 4090 m at Aragats Peak. Cirques form the divide between the basins of the Araxes River to the west and its tributary, the Kasagh, to the east. The divide is marked by both a flat, narrow summit and sharp ridges or rocky peaks (Fig. 10A). The slopes are rocky and steep, with heights ranging from ~200 to 400 m, often cliff-like, and with debris materials forming protalus ramparts, cones, or debris mantles. In this area, glacial erosion traits of varying sizes are frequent (e.g., polished surfaces, striations, roches mouttonnés, etc.), and they are especially noticeable in saddle areas with significant continuity across both slopes. These features indicate the interconnection of ice in the accumulation basins, thus forming a continuous ice mass. On the headwall slopes, several levels of trim lines can be distinguished, located below the highest peaks, showing that ice-free reliefs always existed in the divides between glacial basins. These basins are clearly represented by the large glacial valleys up to ~17 km, along which the ice tongues flowed (Fig. 3, Table 5). These geomorphological features match the identification

criteria of an icefield-type plateau glacier, resulting in the interconnecting of several accumulation zones.

These configurations of the glacial system are clearly indicated by the cirque typologies. Cirques allow us to deduct the morphology of the ancient ice masses in the accumulation basins and their ability to transform previous reliefs. In Mount Aragats, the former icecap sector is characterized by U-shaped cirques (troughs), and the icefield sector by semicircular cirques (concaves) (Fig. 4C). This interdependence between the type of ice masses and the morphology of the cirques can be interpreted as the result of glacial superimposition on the previous volcanic morphology.

Cirque genesis is complex and controlled by multiple factors: (1) preglacial topography, (2) structural geology, (3) glacial history, and (4) regional climate (Unwin, 1973). Initial stages of cirque are associated with ice accumulation in pre-existing hollows of different origin, such as fluvial, gravitational, periglacial, or volcanic (Haynes, 1968; Graf, 1976; Turnbull and Davies, 2006; Sanders et al., 2013). In Mount Aragats, a sequence of staircase smaller cirques has been detected within the larger ones, a configuration that has been termed "cirques within cirques" in other regions (Evans, 2010; Delmas et al., 2015). These smaller cirques are distributed to some extent, randomly and do not form a fractal system as would be expected from a sequence caused by glacial over-deepening processes in stepped terrains (Evans and McClean, 1995; Evans, 2003, 2010). Given that many of these cirques are located close to the main emission centres of the Aragats stratovolcano (Chernyshev et al., 2002) and some of the smaller cirques have horseshoe-shaped contours above the bed of the larger cirque (Fig. 4D), it is likely that preexisting hollows correspond to ancient craters reshaped by the ice. On the other hand, the primary origin of some cirques in former torrential basins, debris flow zones, and lahars formed on the slopes of volcanic cones cannot be ruled out. This hypothesis is supported by the arrangement of glacial valleys and a comparative analysis with certain current stratovolcanoes like Aragats, such as Ararat, Nevado Copurana, Mount Rainier, etc. (Cullen et al., 2006; Campos-Oset, 2012; Churikova et al., 2015; Alcalá-Reygosa et al., 2016; Azzoni et al., 2017; Báez et al., 2020; Samolczyk et al., 2024). These data allow us to consider that the genesis of cirques in Mount Aragats is a combination of multiple factors, such as their preferential location is following the dominant trajectory of regional storms (NW-SE and N-S; Joannin et al., 2014; Nestler et al., 2014; Wegwerth et al., 2021), with the preglacial morphology of volcanic origin (craters and lava flow channels; Chernyshev et al., 2002; Gevorgyan et al., 2020), fluvial and associated processes (e.g., torrents, debris flow, lahars) and the distribution of the maximum elevations.

5.2. *Chrono-evolutionary sequence and correlations*

Using the morphostratigraphic succession, the ^{36}Cl-CRE chronology obtained in this research and the regional correlations, a preliminary model of a complete and complex chrono-evolutionary sequence has been determined in the paleoglaciers of Mount Aragats involving the Penultimate Glacial Cycle the Last Glacial Cycle, and the Post-Glacial Period or Present Interglacial (Fig. 11).

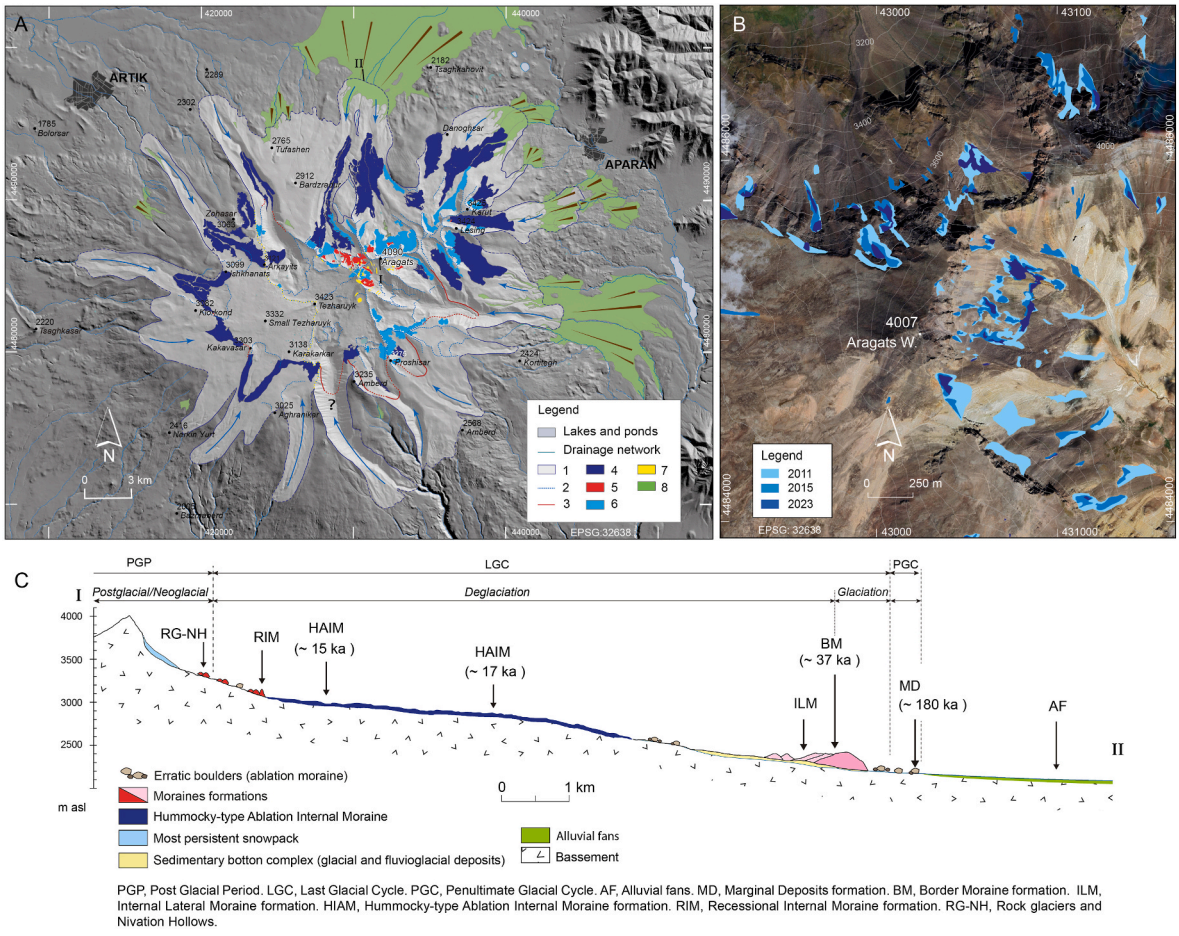

PGP, Post Glacial Period. LGC, Last Glacial Cycle. PGC, Penultimate Glacial Cycle. AF, Alluvial fans. MD, Marginal Deposits formation. BM, Border Moraine formation. ILM, Internal Lateral Moraine formation. HIAM, Hummocky-type Ablation Internal Moraine formation. RIM, Recessional Internal Moraine formation. RG-NH, Rock glaciers and Nivation Hollows.

Fig. 11. A) Main morphostratigraphic and evolutionary indicators of glaciers on Mount Aragats. (1) Contour of maximum ice extent (see Fig. 5); (2) glacial cirques; (3) recessional internal moraines; (4) hummocky-type ablation supraglacial moraine; (5) residual moraine arcs; (6) rock glaciers; (7) most persistent snowpack on Mount Aragats; (8) alluvial fans. B) detailed mapping of the most persistent snowpack on Mount Aragats using a combination of satellite image from Bing, Yandex and Google images in September. C) Simplified geomorphological sketch of glacial landforms and chronology on Mount Aragats glaciations. Interpretation based on longitudinal profile across the Getadzor valley (I-II, see Fig. A).

5.2.1. Penultimate Glacial Cycle (PGC) in Mount Aragats (stage I)

With little discrepancies, PGC was established between c. 200 ka and c. 130 ka, spanning between Termination IIIa and Termination II, corresponding to the MIS6 (Lisiecki and Raymo, 2005; Railsback et al., 2015; Hughes and Gibbard, 2018; Cohen and Gibbard, 2019; Clark et al., 2020; Bardají and Lario, 2022; Hughes, 2022). At Mount Aragats, seven samples collected in the MD formation fall within this time range from c. 181 ka to c.142 ka (Table 4, Fig. 11).

The evidence of pre-LGC glaciations usually appears in marginal areas far from the end of current valleys (isolated erratic boulders, residual and partially fossilized polished surfaces, paleosols, etc.) or in the fluvioglacial deposits of the proglacial domain. In many cases, this has been explained due to the glacial dynamic of the LGC being superimposed over the most direct morphological remains (e.g., polished, valleys, moraines) of previous glaciations (see Palacios et al., 2022). The problems in identifying pre-LGC glaciations on Mount Aragats coincide with those detected in some European mountain ranges where this topic is under permanent discussion, such as the Alps (see Dehnert et al.,

Table 7
Evolutionary sequence of Mount Aragats glaciers and regional correlation.

Glaciation	Location and context
Present-day glaciers in and around the Armenian Highlands.	- Mount Aragats: Last residual glaciers (firn basins). 28 with an area of 2.47 km^2, observed in the years 1975–1976. Davoyan (1971), Tsomaya et al. (1983). - Greater Caucasus Mountain (Russia, Georgia, and Azerbaijan): 2020 plateau, valley and cirque glaciers identified. Glacier inventory of the year 2014. See: Stokes et al. (2006), Solomina et al. (2016, 2022), Tielidze (2017), Tielidze et al. (2020), Tielidze and Wheate (2018). - Western border of Armenian Highland (Turkey). 1-Mount Ararat: Ice cap and outlet glaciers. 2-Mounts Suphän (Sipan) and Asanbesir and Eastern end of the Black Sea Mountains: scattered and residual glacial ice. 3- South-eastern Taurus Mountain (Uludoruk and Dolampar): Residual cirque glaciers. See: Çiner (2004), Sarikaya et al. (2011), Çalışkan et al. (2014), Yavaşlı et al. (2015), Azzoni et al. (2017). - South-eastern border of the Armenian Highland (Iran). Sabalan region: scattered and residual glacial ice. Moussavi et al. (2009).

Glaciation	**Location and context**		**Chronology**	
Ancient glaciers in the Armenian Highlands and surround areas.	Mount Aragats. Relative chronology established by geomorphological data and regional correlations.		By correlation with the Alps, this glaciation has been assigned as equivalent to the Würm (110-10 ka BP; MIS5a to MIS2), that is, to the LGC. The succession of moraines in some glaciers, is correlated with the alpine tardiglacial stadials, Egesen, Daun and Gschnitz and the historical advance Fernau. Boynagryan (2020, 2021).	
	Mount Aragats. Absolute chronology obtained by ^{36}Cl-CRE dating on boulders of moraines.		Two glaciations from the Middle and Late Pleistocene (Carrasco et al. in this paper): I The Penultimate Glacial Cycle (MIS6): (1) Glacial Maximum (c. 180 ka, MIS6e); (2) minor oscillations and retreat with five pulses from c. 180 ka to c 142 ka (c. 177 ka, c. 168 ka, c. 164 ka, c. 160 ka, c. 153 ka; MIS6e to MIS 6a); (3) onset of deglaciation or Termination II (after c. 142 ka, MIS6a). II Last Glacial Cycle (MIS5d-MIS1): (1) Maximum Ice Extent (c. 111 ka, MIS5d); (2) minor oscillations, readvance c. 84 ka (MIS5a) and retreat prior to c. 36 ka (MIS3a); (3) first readvance post MIE and major stabilization stage (c. 36 ka, MIS3a); (4) first stage of deglaciation (after to c 36 ka and prior to 17 ka; between MIS3a and MIS2); (5) second stage of deglaciation and limited readvance followed by a rapid ablation (c. 17 ka, MIS2 correlated to Oldest Dryas Stadial); (6) third and final stage of deglaciation, and the onset of ice-free conditions after a shorth stage of readvance (after to c. 17 ka and estimated prior to transition to the Holocene). III. Postglacial Period (Holocene).	
	Syunik-Vorotan upland (Armenia). Absolute chronologies established in complex sedimentary series (fluvial, glacial, lacustrine, etc.) and volcanic materials.		Several glaciations from the Middle Pleistocene to the present. Specifically, glacial, and fluvioglacial deposits are dated from: MIS12 (478-424 ka, coincident with Termination V), MIS6 (191-130 ka, coincident with the Pre-LGC and the TII) and MIS4 to MIS2 (109- 14 ka, coincident with the LGC). Ollivier et al. (2010).	
	Caucasus Mountain. Chronologies established by lithological, geomorphological and palynological data.		Glaciation correlated with alpine Würm stage. See: Gobejishvili et al. (2011), Revaz et al. (2018), Tielidze (2017).	
	Absolute chronologies established using ^{10}Be and ^{36}Cl-CRE with glacial boulders samples and polis bedrocks in several mountains in Turkey.	Kavron Valley Northwestern Anatolia	Pre-LGC glacial period.	126 ± 5 ka. Akçar et al. (2007). 127 ± 64 ka. Yavuz (2014).
		Kuruova valley in Mt. Akdag, Mt. Soğanlı. Basyayla Valley in the Kackar Mountains Barhal Valley in the Kaçkar Mountains of northeastern Anatolia	MIE prior to and correlative with the LGM.	Glacial advances around 60, 50, 40 and 30 ka. Sarikaya et al. (2014, 2025). Glacial advances around 55, 40 and 30 ka. Reber et al. (2014). Glacial advances around 34, 22 and 18 ka BP, within the global LGM time window. The end of glaciation occurred around 15 ka BP. Reber et al. (2022).
		Kackar Mountain, Eastern Black Sea Mountain range	MIE correlative with the LGM. Other stages and deglaciation.	Glacial advance around 26 ka BP. A second advance around 18 ka BP and a final one between 13-11 ka BP correlative with the Younger Dryas Stadial. Akcar et al. (2007).
		Karçal Mountains, Lesser Caucasus		There are no data on the chronology of the MIE but is interpreted correlatively to LGM (MIS2). The beginning of the deglaciation is about 19 ka BP and the end of the glaciation around 15 ka BP. Dede et al. (2017).
		Mount Karadag, west of the Western Taurus Mountains		MIE around 22.4 ± 2.8 ka during the LGM and advances during the Lateglacial (15.5 ± 2.7 ka) and the Younger Dryas (12.4 ± 1.1 ka). Bayrakdar et al. (2024).

LGC, Last Glacial Cycle. LGM, Last Glacial Maximum (global). MIE, Maximum Ice Extent (local). MIS, Marine isotope stages. T, Termination of the glacial periods or cycles. CRE, Cosmic Ray Exposure Dating using Beryllium 10 or Chlorine 36 isotope.

2010; Dieleman et al., 2022; Ivy-Ochs et al., 2022), Iberian mountains (Oliva et al., 2019, 2022; Fernandes et al., 2021; Vieira et al., 2021; Turu, 2023) or Turkey mountains (Akçar et al., 2007; Yavuz, 2014; Akçar, 2022) (Table 7).

According to these data and following the methodologies already applied in other mountains (Carrasco et al., 2013, 2015, 2023), in this research, special attention was paid to detecting the outermost residual deposits of these glaciers, which represent the absolute maximum and the oldest evolutionary stages. The results obtained show total convergence with the areas previously mentioned: most of the set of glacial morphologies corresponds to the LGC, and the remains of an ancient glaciation have only been detected in some scattered erratic boulders of the MD formation. With the data obtained, it is possible to approximate an evolutionary sequence of this glaciation in three major stages (Fig. 11).

– (I.1) PGC build-up and Inception. The onset to absolute Maximum Ice Extent or Aragats Glacial Maximum (AGM)

The oldest age obtained from the glaciers of Mount Aragats is ~181 (ARG01; MIS 6e) and corresponds to the MD formation (Figs. 3 and 6, Table 4), which represents the "absolute" Maximum Ice Extent of the glaciations in this area and, therefore, should be considered as the Mount Aragats Glacial Maximum (AGM). This age is consistent with the one established in nearby areas at the beginning of PGC (Syunik-Vorotan upland, Armenia; Table 7). According to this data and considering the chronologies established for the start of this glacial cycle (c. 200 ka), it can be interpreted as a gradual process of glacial inception lasting approximately 20 ka.

Due to the superimposition of the glacial morphologies of the LGC on those originating in the PGC, it is difficult to interpret the morphological configuration of the glacier's growth and consolidation in this period. It is assumed that and in this glacial cycle, there was a progressive growth of the ice masses until consolidating a plateau glacier system with valleys that channelled the emissary tongues, reaching several kilometres, similar to that occurring during the LGC.

– (I.2) Ice oscillation and Limited retreat during the PGC. From the Aragats Glacial Maximum (AGM) to the onset of Termination II (TII).

The ages for this evolutionary stage range from c. ~177 ka (ARG10) to c. ~142 ka (ARG19) and correspond to 6 samples that have provided a complete record of all the MIS6 substages proposed for the PGC (Railsback et al., 2015) (Figs. 3 and 6, Table 4). These ages suggest multiple glacial oscillations around the MIE, most likely conditioned by the alternations of colder and warmer substages, as proposed on the MIS scale (see Railsback et al., 2015; Bardají and Lario, 2022; and references). During the penultimate (MIS6) and last (MIS2-4) glacial period, also in this area, such oscillations have been recorded in stalagmites in the Sofular Cave (Turkey) (Held et al., 2024).

The arrangement of the deposits indicating this evolutionary stage (i.e., MD formation) shows that once glaciers reached their maximum extent, they maintained similar dimensions for several evolutionary stages with very slow withdrawal. This relative stagnation and oscillation of the glaciers around their maximum extent (MIE) have been described in numerous mountain ranges worldwide (see Palacios et al., 2022). Considering the results shown in this work and taking into account the proposed age for the start of the TII (c. ~138 ka) (Cheng et al., 2009; Menviel et al., 2019; Clark et al., 2020), the glaciers on Mount Aragats remained at similar dimensions for about 40 ka, between c. 180 ka (oldest age obtained) and c.142 ka (younger age obtained within MIS6).

– (I.3) Onset of PGC Deglaciation stages. Termination II (TII) in Mount Aragats

Globally, the estimate of the onset of TII is around 135–138 ka (Shackleton, 1969; Cheng et al., 2009; Hughes and Gibbard, 2018; Menviel et al., 2019; Clark et al., 2020; Rex et al., 2024). Considering these chronological references, the age of c. ~142 ka (MIS6a) (Table 4), obtained at Mount Aragat would correspond to the onset of the TII and, thus, it might represent the change of glacier trend from the slow to full retreats. Given the position of that sample in the outer zone of the valleys (corresponding to the MD formation; Figs. 3 and 6), it can be established that the deglaciation of this PCG in Mount Aragats was very rapid and in only about 7 ka, the large mass of ice would be lost with the beginning of the Last Interglacial Period (LIP, c. ~130-115 ka).

5.2.2. *Last Glacial Cycle (LGC) in Mount Aragats (stage II)*

The LGC occurred from the end of the Last Interglacial to the beginning of the Holocene (115–11.7 ka; MIS5d to MIS1; and GS-26 to GS-1) (Preusser, 2004; Lisiecki and Raymo, 2005; Railsback et al., 2015; Hughes and Gibbard, 2018; Cohen and Gibbard, 2019; Clark et al., 2020; Bardají and Lario, 2022; Hughes, 2022; Rasmussen et al., 2014). The morphology and chronology of this glacial cycle on Mount Aragats was solved due to the excellent preservation of the morphostratigraphic indicators. Taking this data into account, the evolutionary sequence of this glaciation has been established in the following stages (Fig. 11).

– (II.1) Inception and build-up to the LGC. From the onset to Maximum Ice Extent (MIE-LGC)

The oldest age obtained on the Mount Aragats glaciers for this glaciation is ~111 ka (ARG20; MIS 5d; GI-25b), belonging to the MD formation (Figs. 3 and 6, Table 4). According to this, the glacial maximum of this cycle (MIE-LGC) is significantly earlier than the period of the global Last Glacial Maximum (LGM), set between 29-23 ka (onset) and 19-17 ka (end) according to different authors (see: Mix et al., 2001; Clark et al., 2009; Hughes and Gibbard, 2014; Hughes, 2022). In addition to the data presented below, it allows us to correlate the glaciation of these mountains with those of the Mediterranean Region, in which the glacial maximum and other secondary advances occurred before the LGM (see Hughes and Woodward, 2025 and references). Considering the global chronologies established for the beginning of this glacial cycle (c. 115 ka), it can be interpreted tentatively that in this area, the inception process was very fast, c. 5 ka, which contrasts with the evolution of the previous cycle (PGC).

The growth of the ice masses ends with the development of the large ice plateau of the summits of Mount Aragats and the long glacial tongues of its valleys. In this stage, large masses or ice sheets predominate on the summits, with valleys still poorly defined. This morphological and dynamic context, together with the absence of ice-free reliefs, may explain the scarcity of deposits from this evolutionary stage and the absence of moraine-type stabilization accumulations at the fronts and margins of the glaciers.

– (II.2) Ice oscillation and Limited retreat. From MIE-LGC to Mayor Stabilization

The only numerical age obtained at this evolutionary stage corresponds to an erratic boulder of the MD formation that provided an age of c. ~84 ka (ARG12; MIS5a; GI-21.1e). Considering to the arrangement of the morphostratigraphic units and the corresponding chronologies, this stage of oscillations around the maximum (MIE-LGC) indeed extended for about 27 ka between c.~111 ka to ~84 ka (MIS5d and 5a; samples ARG12 and ARG20; Figs. 3 and 6, Table 4).

As in the PGC, the arrangement of the deposits indicating this evolutionary stage (i.e., MD formation) shows that once glaciers reached their maximum extension, they maintained similar dimensions during several evolutionary stages with very slow retreats. Although, according to the available indicators (i.e., deposits, trim lines, polished surfaces free of ice), the magnitude of the retreat of the ice was minimal, its

effects were notable in the availability of ice-free walls capable of providing debris to the glacier, enabling the formation of large moraines.

– (II.3) Major stabilization and first readvance post MIE-LGC

The indicator of this evolutionary stage is the most prominent lateral moraine (i.e., BM formation) that defines the external limit of the valleys. The only quantitative chronology obtained at this evolutionary stage corresponds to a moraine boulder of the BM formation that provided an age of c. ~37 ka (ARG18; MIS3a; GI-8b). This glacial advance in the Mount Aragats area is statistically asynchronous with the LGM and with other chronologies obtained in the Armenian Highlands (Syunik-Vorotan upland) and some mountains of Turkey (Kackar, Karçal and Karadag mountains). However, there is a remarkable convergence with the stages obtained in nearby areas of the same mountains of Turkey (Kuruova, Basyayla and Barhal valleys) (Table 7).

After the previous stages of limited retreat, the ice began to stabilize and, according to all the evidence, is the largest of the entire glaciation and includes glacial advances sometimes referred to as the "second LGM" (see Carrasco et al., 2015 and references). This stage has been detected in numerous European mountains and the Mediterranean region, although in these areas it has usually been associated with MIS 2 (see Palacios et al., 2022). However, it presents a certain age dispersion, and it is often described as an asynchronous stage, even between very close areas (López-Moreno and García-Ruiz, 2024).

The time of construction of this BM formation is after c. 84 ka up to c. 37 ka, as indicated by the age of the last deposits of the MD formation and that of the main ridge of these moraines. This means that this evolutionary stage could have lasted from the MIS5e or MIS4 to the end of MIS3, i.e., more than 40 ka.

Although more attenuated, the changes initiated in the previous stage continue, allowing the progressive definition of the glacial tongues and their corresponding moraines in front of the ice sheets and block fields. The glacial retreat initiated in the previous stage leaves some walls free of ice, favouring decompression processes (debuttressing) and a notable increase in supraglacial debris. This process involved the construction of large lateral moraines and valleys, which were increasingly better defined by glacial excavations that constricted and channeled the ice masses.

– (II.4) Onset of Last Deglaciation or Termination I on Mount Aragats (TI). Major retreat.

Although there are no numerical data for this evolutionary stage, based on the morpho-stratigraphic succession, deducing its position and evolutionary context is possible. The previous stabilization stage ended with an abrupt change of trend and the beginning of a new glacial retreat, which caused the ice masses to decrease, leaving them embedded in the valleys limited by the moraines of the BM formation. This process occurred through a sequence of pulsations interrupted by short stages of stabilization, which allowed the formation of minor moraines attached to the BM that constitute the ILM formation.

Given that the ice masses would no longer reach the previous extensions, this stage can be considered the beginning of deglaciation or TI on Mount Aragats. According to chronologies obtained, this evolutionary stage can be limited between the c. ~37 ka (age of MB, previous formation) and the c. ~17 ka (age of HAIM, subsequent formation) and spanning the end of MIS3 and most of the MIS2. Considering chronologies proposed for the onset of global TI (c. 19 ka; MIS2, GS-2.1b) (see Palacios et al., 2023; Denton et al., 2010; Clark et al., 2020), Mount Aragats show a notable asynchronicity compared to the equivalent global estimates (Schaefer et al., 2006).The potential glacier demise process in the Mount Aragats region is in line with archaeological data indicating a notable change in human activity occurred in the area between 24 and 20 ka within MIS2 (Malinsky-Buller et al., 2024; Wolf et al., 2022, 2024).

– (II.5) Second stage of TI. Limited readvance followed by a large retreat with rapid ablation.

Two samples of boulders from the moraines HAIM have provided ages of c. ~17 ka (ARG-22) and ~15 ka (ARG-08). Therefore, this evolutionary stage can be placed in the context of the Oldest Dryas stadial or Heinrich Event 1 (c.17–14.5 ka; MIS2, GS-2.1a). This chronology is equivalent to that obtained by Çiner et al. (2015), Altınay et al. (2024), and Sarikaya et al. (2025) in the Central Taurus Mountain Range and Davraz (Turkey), respectively, applying ^{36}Cl-CRE on hummocky-type formations like Mount Aragats.

Great activity on the slopes gives rise to debris-covered glaciers that slightly advance over the previous formations. Rapid retreat and formation of hummocky-type ablation moraines (HAIM formation) that, in some areas, overlap and fossilize moraines of the prior stage (ILM). Due to this activity on the slopes and the progressive disconnection of the ice masses, the development of some rock glaciers attached to the slopes started at this stage (talus rock glacier-type; see Ballantyne, 2024).

– (II.6) Third and final stage of TI. Minors readvance, stabilization and disappearance of the glaciers in the valleys.

There are no quantitative chronologies for this evolutionary stage either, but in this case, it is possible to deduce its position and evolutionary context from the morphostratigraphic succession. This stage begins with the final consolidation of the hummocky moraine and a slight recovery of the ice masses that quickly gives way to a general retreat and disappearance of the glaciers in the valleys, remaining limited to the cirques. Both stages can correlate with the Older Dryas cold pulse (c. 14–13.9 ka; MIS1, GI-1d) and the Alleröd interstadial (13.9–12.8 ka; MIS1, GI-1a-1b-1c). The ice continued to retreat in some glaciers, giving way to small nivation hollows and cirque rock glaciers. However, in others, the ice stabilized and even experienced a notable recovery, forming the arcuate moraines (RIM formation) indicative of a cold stage of glacier readvance that can correlate with the Younger Dryas stadial (c. 12.8–11.6 ka; MIS1, GS-1).

5.2.3. Post-Glacial Period (PGP) in Mount Aragats (stage III)

– (III.1) End of glaciation and Neoglacial advance.

There is no clear evidence of Neoglacial glacier activity in Mount Aragats. The most recent quantitative age obtained in this area is c. ~10 ka (ARG25) post-glacial (MIS1; Early Holocene). However, it corresponds to a boulder of the HAIM formation very far from the head of the valleys and presents a discrepancy with the morphostratigraphic sequence defined in this work due to possible distortions in the dating by post-glacial toppling of the boulder or erosion of its surface, so it must be considered as an outlier (Figs. 3 and 6, Table 4).

As previously discussed, there is currently no data available to establish the precise age of the onset of TI on Mount Aragats. However, a date obtained by ^{14}C dating of the sediments of Unroy glacial lake close to the headwall of Mount Aragats indicates that large glaciers would have already disappeared about 7000 years ago (Sapelko et al., 2019; Sevastyanov et al., 2021).

The remarkable increase of ice-free terrain in this evolutionary stage resulted in a significant expansion of peri- and paraglacial processes activity originating in remarkable debris talus and mantles, as well as protalus and talus rock glaciers. During the Holocene cold pulses, rock glaciers were developed in the bed of cirques, névè moraines and arcuate moraines of residual cirque glaciers. The latter was especially significant in the Fernau or Little Ice Age pulse and persisted until the second half of the 20th century as firn basins, which have been considered the last glaciers observed on Mt. Aragats (Davoyan, 1971;

Tsomaya et al., 1983; Boynagryan, 2020, 2021) (Figs. 4 and 11).

– (III.2) Current stage. Significant retreat of snow cover.

Current observations allow us to establish a total retreat of snow and perennial ice (firn basins). However, there are active rock glaciers, some névè moraines and great activity of slope processes such as debris flow and debris slides (Figs. 4 and 11).

6. Conclusions

According to our research, centrifugal-type plateau glaciers were developed during the Middle and Upper Pleistocene (from MIS6e to MIS1) on Mount Aragats with valley radiating from the summits to the piedmonts, in two configurations: icecap type in the western area with flat-topped topography and icefield type in the eastern region with sharp-topped topography. During the Maximum Ice Extent (MIE) in the Mounts Aragats area, 19 glaciers have been identified with a total length (tongue and cirque) of up to ~17 km, characterized by tongues with ice thicknesses of up to ~350 m and some glaciers that descended from about 3900 masl to 2040 masl (Fig. 3, Table 5).

Multiple moraines were identified, generally forming accretion sequences and exceptionally superimposed sequences. These moraines indicate stages of ice advance, stagnation or stabilization and retreat. The materials forming these moraines are massive diamictons, and occasionally structured, comprising the three basic types of till deposits: supraglacial melt-out, subglacial melt-out and lodgment.

According to morpho-stratigraphic succession of the moraines, absolute chronologies and regional correlations, the chrono-evolutionary sequence of these glaciers can be established in three cycles (Fig. 11): (I) the Penultimate Glacial Cycle (PGC; MIS6), (II) Last Glacial Cycle (LGC; MIS5d-MIS1) and (III) the Post-Glacial Period (PGP, Holocene, MIS1).

(I) The PGC is indicated by the Marginal Deposit Formation (MD) and comprises (1) the early stages of glaciation of Mount Aragats from the onset to the Maximum Ice Extent or absolute Glacial Maximum on Mount Aragats (AGM; c. 180 ka, MIS6e); (2) minor oscillations around the MIE-ARGM position and retreat with potentially five pulses from c. 180 ka to c 142 ka (c. 177 ka, c. 168 ka, c. 164 ka, c. 160 ka, c. 153 ka; MIS6e to MIS 6a); and (3) the onset of deglaciation or Termination II (after c. 142 ka, MIS6a).

(II.A) The LGC during the period of glaciation includes: (1) from the onset to Maximum Ice Extent (LGC-MIE; c. 111 ka, MIS5d); (2) minor oscillations around MIE position, readvance c. 84 ka (MIS5a) followed by limited retreat pulse (prior to c. 36 ka, MIS3a); and (3) second LGC-advance and major stabilization stage (c. 36 ka, MIS3a). Stages 1 and 2 are indicated by the outermost deposits (MD formation) and three by large lateral moraines (BM formation).

(II.B) The LGC during the period of deglaciation includes: (4) a first stage of deglaciation and major retreat indicated by minor internal lateral moraines (ILM formation; after to c 36 ka and prior to 17 ka; between MIS3a and MIS2); (5) a second stage of deglaciation and limited readvance (second readvance post MIE or third LGC-advance) followed by a large retreat with rapid ablation indicated by the hummocky-type ablation internal moraines (HAIM formation; c. 17 ka, MIS2 correlated to Oldest Dryas Stadial); (6) a third and final stage of deglaciation, general retreat and the onset of ice-free conditions after a short stage of readvance indicated by arcuate recessional internal moraines (RIM formation; after to c. 17 ka and estimated before transition to the Holocene).

(III) The PGP is represented by active rock glaciers, some arcuate moraines of residual glaciers, névè moraines and great activity of slope processes such as debris flow and debris slides.

Finally, it can also be concluded that the evolution of the glaciation of Mount Aragats is comparable with those described in the Mediterranean Region: here, too, the penultimate (PGC) and last (LGC) glacial cycles and several LGC-advances prior to the LGM have been identified.

Author contributions

Rosa M. Carrasco: coordination, mapping, data processing, wrote the paper with contributions from all coauthors, review and editing. Javier Fernández-Lozano, Theodoros Karampaglidis, Rodrigo L Soteres, and Javier Pedraza: data processing, writing, editing and revision. Ré; gis Braucher and Stéphanie Gairoard: CRE chronology, writing and revision. Artur Petrosyan, Samvel Nahapetyan, Dmitri Arakelyan and Boris Gasparyan: writing and revision.

Declaration of competing interest

The authors declare that they have no known competing financial interests or personal relationships that could have appeared to influence the work reported in this paper.

Acknowledgements

This research is part of the project reference PID2020-117685 GB-I00 funded by MCIU/AEI/10.13039/501100011033 and the project funded by the grant reference 2022-GRIN-34112 and the European Regional Development Fund (ERDF). Partial funding also comes from ANID FONDECYT postdoctoral grant #3220537, the ANID BASAL CHIC #FB210018 and the ANID FONDECYT Regular #1220550. The authors also wish to acknowledge the Universidad de Castilla-La Mancha and the Dirección General de Juventud y Deportes (Junta de Comunidades de Castilla-La Mancha) for their collaboration and support in the TransCause-2024 Conference held in Toledo (Spain). The authors would also like to thank the Institute of Archaeology and Ethnography for supporting the project and preparing all necessary permits for the fieldwork and sample transport from the Higher Education and Science Committee, Republic of Armenia, under grant number 21AG-6A080. Finally, we also thank the Editor and reviewers, for their helpful comments and constructive suggestions that greatly improved this manuscript.

ASTER AMS, a national facility (CEREGE, Aix en Provence), is supported by the INSU/CNRS and IRD and members of AIX MARSEILLE PLATFORMS and REGEF networks.

Data availability

All data and/or code is contained within the submission.

References

Abich, H., 1882. Geologie des Armenischen Hochlandes 2. A. Hölder.

Akçar, N., 2022. The Anatolian mountains: glacial landforms prior to the Last Glacial Maximum. In: Palacios, D., Hughes, P.D., García-Ruiz, J.M., Andrés, N. (Eds.), European Glacial Landscapes. Maximum Extent of Glaciations. Elsevier, pp. 333–337. https://doi.org/10.1016/B978-0-12-823498-3.00027-3.

Akçar, N., Yavuz, V., Ivy-Ochs, S., Kubik, P.W., Vardar, M., Schlüchter, C., 2007. Paleoglacial records from Kavron valley, NE Turkey: field and cosmogenic exposure dating evidence. Quat. Int. 164–65, 170–183. https://doi.org/10.1016/j.quaint.2006.12.020.

Akçar, N., Ivy-Ochs, S., Kubik, P.W., Schlüchter, C., 2011. Post-depositional impacts on 'Findlinge' (erratic boulders) and their implications for surface-exposure dating. Swiss J. Geosci. 104, 445–453. https://doi.org/10.1007/s00015-011-0088-7.

Altınay, O., Sarıkaya, M.A., Wilcken, K.M., 2024. A rare piedmont glaciation in the Mediterranean: insights from cosmogenic ^{36}Cl dating of Davraz hummocky moraine field (SW Türkiye). Earth Surf. Process. Landf. 49 (7), 2047–2066. https://doi.org/10.1002/esp.5815.

Alcalá-Reygosa, J., Palacios, D., Zamorano-Orozco, J.J., 2016. Geomorphology of the Ampato volcanic complex (southern Peru). J. Maps 12 (5), 1160–1169. https://doi.org/10.1080/17445647.2016.1142479.

Arimura, M., Gasparyan, B., Chataigner, C., 2012. Prehistoric sites in northwest Armenia: Kmlo-2 and Tsaghkahovit. In: Matthews, R., Curtis, J. (Eds.), Proceedings of the 7th

International Congress of the Archaeology of the Ancient Near East, 12 April -16 April 2010, the British Museum and UCL, London, Volume 3: Fieldwork and Recent Research Posters. Harrassowitz Verlag, Wiesbaden, pp. 135–139.
Athanassas, C.D., Bourlès, D.L., Braucher, R., Druitt, T.H., Nomikou, P., Léanni, L., 2016. Evidence from cosmic-ray exposure (CRE) dating for the existence of a pre-Minoan caldera on Santorini, Greece. Bull. Volcanol. 78, 35. https://doi.org/10.1007/s00445-016-1026-3.
Azzoni, R.S., Zerboni, A., Pelfini, M., Garzonio, C.A., Cioni, R., Meraldi, E., Smiraglia, C., Diolaiuti, G.A., 2017. Geomorphology of Mount Ararat/Ağri Dağı (Ağri Dağı Milli Parki, eastern Anatolia, Turkey). J. Maps 13 (2), 182–190. https://doi.org/10.1080/17445647.2017.1279084.
Badalyan, R.S., Avetisyan, P.S., 2007. "Bronze and Early Iron Age Archaeological Sites in Armenia", I, Mt. Aragats and its Surrounding Region, vol. 1697. Bar International Series, Oxford.
Ballantyne, C.K., 2024. Talus rock glaciers in the Cairngorm mountains. Scott. Geogr. J. https://doi.org/10.1080/14702541.2024.2321880.
Bardají, T., Lario, J., 2022. Estadios Isotópicos Marinos. Estratigrafía de los isótopos del oxígeno. Cuartenario y Geomorfología 36 (3–4), 143–154. https://doi.org/10.17735/cyg.v36i3-4.94172.
Barr, I.D., Spagnolo, M., 2015. Glacial cirques as palaeoenvironmental indicators: their potential and limitations. Earth Sci. Rev. 151, 48–78.
Báez, A.D., Báez, W., Caselli, A.T., Martini, M.A., Sommer, C.A., 2020. The glaciovolcanic evolution of the copahue volcano, andean southern volcanic zone, Argentina-Chile. J. Volcanol. Geoth. Res. 396. https://doi.org/10.1016/j.jvolgeores.2020.106866.
Bayrakdar, C., Çılğın, Z., Sarış, F., Yeşilyurt, S., Keserci, F., Büyükdeniz, Y., Halis, O., Vockenhuber, C., Ivy-Ochs, S., Akçar, N., 2024. Late Pleistocene glacial history of Mount Karadağ, SW Türkiye. Geomorphology 467. https://doi.org/10.1016/j.geomorph.2024.109467.
Benn, D.I., Ballantyne, C.K., 2005. Palaeoclimatic reconstruction from loch lomond readvance glaciers in the west drumochter hills, Scotland. J. Quat. Sci. 20, 577–592. https://doi.org/10.1002/jqs.925.
Benn, D.I., Evans, D.J.A., 2010. Glaciers & Glaciation. Hodder Education, second ed., p. 802 London.
BI, 2024. Bing Maps Dev Center. Microsoft Corporation. https://www.bingmapsportal.com/.
Boynagryan, V.R., 2020. Ancient and present-day glaciation of the republic of Armenia. Proceedings of the YSUC: Geological and Geographical Sciences 54 (2), 99–107. https://doi.org/10.46991/PYSU:C/2020.54.2.099 (In Russ.).
Boynagryan, V.R., 2021. New data of the ancient and modern glaciation of the Armenian Highland. Proceedings of the YSU C: Geological and Geographical Sciences 55 (1), 17–25. https://doi.org/10.46991/PYSU:C/2021.55.1.017 (In Russ.).
Çalışkan, O., Gürgen, G., Yılmaz, E., Yeşilyurt, S., 2014. Debris-covered glaciers during glacial and interglacial periods on the Taurus mountains (Turkey). Procedia Soc Behav Sci 120, 716–721. https://doi.org/10.1016/j.sbspro.2014.02.154.
Campos-Oset, N., 2012. Glacier Evolution in the South-West Slope of Nevado Coropuna (Cordillera Ampato, Perú). Complutense University, Madrid, p. 55. Master Thesis. https://hdl.handle.net/20.500.14352/46588.
Carrasco, R.M., Pedraza, J., Domínguez-Villar, D., Villa, J., Willenbring, J.K., 2013. The plateau glacier in the Sierra de Bejar (Iberian Central System) during its maximum extent. Reconstruction and chronology. Geomorphology 196, 83–93. https://doi.org/10.1016/j.geomorph.2012.03.019.
Carrasco, R.M., Pedraza, J., Domínguez-Villar, D., Willenbring, J.K., Villa, J., 2015. Sequence and chronology of the Cuerpo de Hombre paleoglacier (Iberian Central System) during the last glacial cycle. Quat. Sci. Rev. 129, 163–177. https://doi.org/10.1016/j.quascirev.2015.09.021.
Carrasco, R.M., Soteres, R.L., Pedraza, J., Fernández-Lozano, J., Turu, V., López-Sáez, J. A., Karampaglidis, T., Granja-Bruña, J.L., Muñoz-Martín, A., 2020. Glacial geomorphology of the high Gredos massif: gredos and pinar valleys (Iberian central system, Spain). J. Maps 16 (2), 790–804. https://doi.org/10.1080/17445647.2020.1833768.
Carrasco, R.M., Turu, V., Soteres, R.L., Fernández-Lozano, J., Karampaglidis, T., Rodés, A., Ros, X., Andrés, N., Granja-Bruña, J.L., Muñoz-Martín, A., López-Sáez, J. A., Braucher, R., Pedraza, J., Palacios, D., ASTER Team, 2023. The Prados del Cervunal morainic complex: Evidence of a MIS 2 glaciation in the Iberian Central System synchronous to the global LGM. Quat. Sci. Rev. 312 (1–23), 108169. https://doi.org/10.1016/j.quascirev.2023.108169.
Chandler, B., Lovell, H., Boston, C.M., Lukas, S., Barr, I.D., Benediktsson, Í.Ö., Benn, D.I., Clark, C.D., Darvill, C.M., Evans, D.J.A., Ewertowski, M.W., Loibl, D., Margold, M., Otto, J.-C., Roberts, D.H., Stokes, C.R., Storrar, R.D., Stroeven, A.P., 2018. Glacial geomorphological mapping: a review of approaches and frameworks for best practice. Earth Sci. Rev. 185, 806–846. https://doi.org/10.1016/j.earscirev.2018.07.015.
Charpentier, J., 1823. Essai sur la Constitution Geognostique des Pyrenees. Paris.
Charton, J., 2024. Reconstruction paléoclimatique depuis les derniers 40000 ans à partir de chronologies glaciaires sur l'archipel Kerguelen, établies à l'aide du nucléide cosmogénique chlore-36. Aix Marseille Université, Marseille. PhD dissertation.
Cheng, H., Edwards, L., Broecker, W.S., Denton, G.H., Kong, X., Wang, Y., Zhang, R., Wang, X., 2009. Ice age terminations. Science 326, 248–252.
Chernyshev, V., Lebedev, V.A., Arakelyants, M.M., Jrbashyan, R.T., Gukasyan, Y.G., 2002. Quaternary geochronology of the Aragats volcanic center, Armenia: evidence from k-ar dating. Dokl. Earth Sci. 384 (4), 393–398.
Churikova, T.G., Gordeychik, B.N., Edwards, B.R., Ponomareva, V.V., Zelenin, E.A., 2015. The Tolbachik volcanic massif: a review of the petrology, volcanology and eruption history prior to the 2012-2013 eruption. J. Volcanol. Geoth. Res. 307, 3–21. https://doi.org/10.1016/j.jvolgeores.2015.10.016.
Çilğin, Z., Bayrakdar, C., 2018. Morphometric characteristics of the glacial cirques on Mount Dedegöl. J. Geogr. 36, 27–48. https://doi.org/10.26650/jgeog411356 (In Turkish).
Çilğin, Z., Bayrakdar, C., 2020. Morphometric characteristics of the glacial cirques in the teke Peninsula, southwestern Anatolia. Turk. Geogr. Rev. 74, 107–121. https://doi.org/10.17211/tcd.729978 (In Turkish).
Çilğın, Z., Evans, I.S., Keserci, F., Canpolat, E., Bayrakdar, C., 2024. Morphometric characteristics of glacial cirques and former glaciers in the Geyik Mountains, Western Taurus, Türkiye. Geomorphology 467. https://doi.org/10.1016/j.geomorph.2024.109474.
Çiner, A., 2004. Turkish glaciers and glacial deposits. In: Ehlers, J., Gibbard, P.L. (Eds.), Quaternary Glaciations: Extent and Chronology, vol. 2. Elsevier Publishers, Amsterdam, pp. 419–429. https://doi.org/10.1016/S1571-0866(04)80093-9. Part I: Europe.
Çiner, A., Sarikaya, M.A., Yildirim, C., 2015. Late Pleistocene piedmont glaciations in the Eastern Mediterranean; insights from cosmogenic 36Cl dating of hummocky moraines in southern Turkey. Quat. Sci. Rev. 116, 44–56. https://doi.org/10.1016/j.quascirev.2015.03.017.
Clark, P.U., Dyke, A.S., Shakun, J.D., Carlson, A.E., Clark, J., Wohlfarth, B., Mitrovica, J. X., Hostetler, S.W., McCabe, A.M., 2009. The last glacial maximum. Science 325, 710–714. https://doi.org/10.1126/science.1172873.
Clark, P.U., He, F., Golledge, N.R., Mitrovica, J.X., Dutton, A., Hoffman, J.S., Dendy, S., 2020. Oceanic forcing of penultimate deglacial and last interglacial sea-level rise. Nature 577, 660–664. https://doi.org/10.1038/s41586-020-1931-7.
Colonge, D., Jaubert, J., Nahapetyan, S., Ollivier, V., Arakelyan, D., Devilder, G., Fourlobey, C., Jamois, M.-H., Gasparian, B., Chataigner, C., 2013. Le Paléolithique Moyen De La Haute Valée du Kasakh (Arménie): Caractérisation technologique et peuplement de montage. Paleorient 39 (n°2), 109–140. https://doi.org/10.3406/paleo.2013.5523.
Cohen, K.M., Gibbard, P.I., 2019. Global chronostratigraphical correlation table for the last 2.7 million years, version 2019 QI-500. Quat. Int. 500, 20–31. https://doi.org/10.1016/j.quaint.2019.03.009.
Cullen, N.J., Mölg, T., Kaser, G., Hussein, K., Steffen, K., Hardy, D.R., 2006. Kilimanjaro Glaciers: recent areal extent from satellite data and new interpretation of observed 20th century retreat rates. Geophys. Res. Lett. 33. https://doi.org/10.1029/2006GL027084.
Davoyan, M.O., 1971. Area of modern glaciation on Mt. Aragats and the diminution of firn basins. Int. Geol. Rev. 13 (4), 530–533. https://doi.org/10.1080/00206817109475464.
Dede, V., Çiçek, İ., Sarıkaya, M.A., Çiner, A., Uncu, L., 2017. First cosmogenic geochronology from the lesser Caucasus late Pleistocene glaciation and rock glacier development in the Karçal valley, NE Turkey. Quat. Sci. Rev. 164, 54–67. https://doi.org/10.1016/j.quascirev.2017.03.025.
Dehnert, A., Preusser, F., Kramers, J.D., Akçar, N., Kubik, P.W., Reber, R., Schlüchter, C., 2010. A multidating approach applied to proglacial sediments attributed to the Most Extensive Glaciation of the Swiss Alps. Boreas 39, 620–632. https://doi.org/10.1111/j.1502-3885.2010.00146.x.
Delmas, M., Gunnell, Y., Calvet, M., 2015. A critical appraisal of allometric growth among alpine cirques based on multivariate statistics and spatial analysis. Geomorphology 228, 637–652.
Demek, J. (Ed.), 1972. Manual of Detailed Geomorphological Mapping. IGU Commission for Geomorphological Mapping. Academia, Prague.
Denton, G.H., Anderson, R.F., Toggweiler, J.R., Edwards, R.L., Schaefer, J.M., Putnam, A. E., 2010. The last glacial termination. Science 328 (5986), 1625–1656. https://doi.org/10.1126/science.1184119.
Dieleman, C., Christl, M., Vockenhuber, C., Gautschi, P., Graf, H.R., Akçar, N., 2022. Age of the most extensive glaciation in the Alps. Geosciences 12, 39. https://doi.org/10.3390/geosciences12010039.
Doneus, M., 2013. Openness as visualization technique for interpretative mapping of airborne lidar derived digital terrain models. Remote Sens. 5 (12), 6427–6442.
Dortch, J.M., Owen, L.A., Caffe, M.W., 2013. Timing and climatic drivers for glaciation across semi-arid western Himalayan-Tibetan orogen. Quat. Sci. Rev. 78, 188–208. https://doi.org/10.1016/j.quascirev.2013.07.025.
Evans, I.S., 1977. World-wide variations in the direction and concentration of cirque and glacier aspects. Geogr. Ann. 59A (3–4), 151–175.
Evans, I.S., 2003. Scale-specific landforms and aspects of the land surface. In: Evans, I.S., Dikau, R., Tokunaga, E., Ohmori, H., Hirano, M. (Eds.), Concepts and Modelling in Geomorphology: International Perspectives. Terrapub. Tokio, pp. 61–84.
Evans, I.S., 2010. Allometry scaling and scale-specificity of cirques, landslides and other landforms. Trans. Jpn. Geomorphol. Union 31 (2), 133–153.
Evans, I.S., 2012. Geomorphometry and landform mapping: what is a landform? Geomorphology 137 (1), 94–106. https://doi.org/10.1016/j.geomorph.2010.09.029.
Evans, I.S., Cox, N.J., 1974. Geomorphometry and the operational definition of cirques. Area 6, 150–153.
Evans, I.S., McClean, C.J., 1995. The land surface is not unifractal: variograms, cirque scale and allometry. Z. Geomorphol. - Suppl. 101, 127–147.
Evans, I.S., Çılğın, Z., Bayrakdar, C., Canpolat, E., 2021. The form, distribution and palaeoclimatic implications of cirques in southwest Turkey (Western Taurus). Geomorphology 391. https://doi.org/10.1016/j.geomorph.2021.107885.
Federal Geographic Data Committee (FGDC), 2006. FGDC Digital Cartographic Standard for Geologic Map Symbolization. Federal Geographic Data Committee Document Number FGDC-STD-013-2006, Reston, VA, p. 290, 2 plates. https://ngmdb.usgs.gov/fgdc_gds/geolsymstd/fgdc-geolsym-all.pdf.

Fernández-Lozano, J., Gutiérrez-Alonso, G., 2016. Improving archaeological prospection using localized UAVs assisted photogrammetry: an example from the Roman Gold District of the Eria River Valley (NW Spain). J. Archaeol. Sci.: Reports 5, 509–520.
Fernandes, M., Oliva, M., Vieira, G., Palacios, D., Fernández-Fernández, J.M., Delmas, M., García-Oteyza, J., Schimmelpfennig, I., Ventura, J., ASTER Team, 2021. Maximum glacier extent of the penultimate glacial cycle in the upper Garonne basin (Pyrenees): new chronological evidence. Environ. Earth Sci. 80, 796. https://doi.org/10.1007/s12665-021-10022-z.
Feruglio, V., Khechoyan, A., Gasparyan, B., Chataigner, C., 2005. The geghamavan-1 painted shelter, Aragatsotn province, republic of Armenia. International Newsletter on Rock Art (INORA) 41, 1–7.
Fink, D., Vogt, S., Hotchkis, M., 2000. Cross-sections for ^{36}Cl from Ti at Ep=35–150 MeV: applications to in-situ exposure dating. Nucl. Instrum. Methods Phys. Res. Sect. B Beam Interact. Mater. Atoms 172 (1–4), 861–866. https://doi.org/10.1016/S0168-583X(00)00200-7.
Foster, D., Brocklehurst, S.H., Gawthorpe, R.L., 2008. Small valley glaciers and the effectiveness of the glacial buzzsaw in the northern Basin and Range, USA. Geomorphology 102, 624–639.
Frye, J.C., Willman, H.B., 1962. Morphostratigraphic units in Pleistocene stratigraphy. American Association of Petroleum Petrologists Bulletin 46, 112–113. https://doi.org/10.1306/BC743763-16BE-11D7-8645000102C1865D.
Gasparyan, B., Glauberman, Ph, 2022. Beyond European boundaries: neanderthals in the Armenian highlands and the Caucasus, chapter 15. In: Ramagnoli, F., Rivals, F., Benazzi, S. (Eds.), Updating Neanderthals, Understanding Behavioural Complexity in the Late Middle Palaeolithic. Academic Press, Elsevier Inc., pp. 275–301. https://doi.org/10.1016/B978-0-12-821428-2.00018-4. ISBN 978-0-12-821428-2.
Gevorgyan, H., Repstock, A., Schulz, B., Meliksetian, K., Breitkreuz, C., Israyelyan, A., 2018. Decoding a post-collisional multistage magma system: the Quaternary ignimbrites of Aragats stratovolcano, western Armenia. Lithos 318, 267–282.
Gevorgyan, H., Breitkreuz, C., Meliksetian, K., Israyelyan, A., Ghukasyan, Y., Pfänder, J. A., Sperner, B., Miggins, D.P., Koppers, A., 2020. Quaternary ring plain-and valley-confined pyroclastic deposits of Aragats stratovolcano (Lesser Caucasus): lithofacies, geochronology and eruption history. J. Volcanol. Geoth. Res. 401, 106928.
Gobejishvili, R., Lomidze, N., Tielidze, L., 2011. Late Pleistocene (Würmian) glaciations of the Caucasus. In: Ehlers, J., Gibbard, P.L., Hughes, P.D. (Eds.), Quaternary Glaciations: Extent and Chronology, vol. 15. Elsevier, Amsterdam, pp. 141–147. https://doi.org/10.1016/B978-0-444-53447-7.00012-X. Chap. 12.
Gordon, J.E., 1977. Morphometry of cirques in the Kintail-Affric-Cannich area of Northwest Scotland. Geogr. Ann. 59A, 177–194.
Graf, W.L., 1976. Cirques as glacier locations. Arct. Antarct. Alp. Res. 8, 79–90.
Halama, R., Meliksetian, K., Savov, I.P., Sugden, P.J., Sokół, K., 2020. Pinched between the plates: Armenia's voluminous record of volcanic activity. Geol. Today 36 (3), 101–108.
Hambrey, M.J., Huddart, D., Bennett, M.R., Glasser, N.F., 2011. Genesis of 'hummocky moraines' by thrusting in glacier ice: evidence from Svalbard and Britain. J. Geol. Soc. 154, 623–632. https://doi.org/10.1144/gsjgs.154.4.0623. London.
Haynes, V.M., 1968. The influence of glacial erosion and rock structure on corries in Scotland. Geogr. Ann. 50A, 221–234.
Held, F., Cheng, H., Edwards, R.L., Tüysüz, O., Koç, K., Fleitmann, D., 2024. Dansgaard-Oeschger cycles of the penultimate and last glacial period recorded in stalagmites from Türkiye. Nature communication 15 (1183), 1–9. https://doi.org/10.1038/s41467-024-45507-5.
Hughes, P.D., 2010. Geomorphology and Quaternary stratigraphy: the roles of morpho-, litho-, and allostratigraphy. Geomorphology 123, 189–199. https://doi.org/10.1016/j.geomorph.2010.07.025.
Hughes, P.D., 2022. Concept and global context of the glacial landforms prior to the Last Glacial Maximum. In: Palacios, D., Hughes, P.D., García-Ruiz, J.M., Andrés, N. (Eds.), European Glacial Landscapes. Maximum Extent of Glaciations. Elsevier, pp. 197–199. https://doi.org/10.1016/B978-0-12-823498-3.00057-1. Chap. 27.
Hughes, P.D., Gibbard, P.L., 2014. A stratigraphical basis for the last glacial maximum (LGM). Quat. Int. 383, 174–185. https://doi.org/10.1016/j.quaint.2014.06.006.
Hughes, P.D., Gibbard, P.L., 2018. Global glacier dynamics during 100 ka Pleistocene glacial cycles. Quat. Res. 90, 222–243. https://doi.org/10.1017/qua.2018.37.
Hughes, P.D., Woodward, J.C., 2025. Middle and late Pleistocene glacial history of the mediterranean mountains. In: Elias, S. (Ed.), Encyclopedia of Quaternary Science, third ed. Elsevier, pp. 674–690. https://doi.org/10.1016/B978-0-323-99931-1.00269-5. vol. 2.
Imagery, 2017. World Imagery. ArcGIS Online. ESRI.
Ivy-Ochs, S., 2015. Glacier variations in the European Alps at the end of the last glaciation. Cuadernos de Investigación Geográfica 41, 295–315. https://doi.org/10.18172/cig.2750.
Ivy-Ochs, S., Monegato, G., Reitner, J.M., 2022. The Alps: glacial landforms prior to the last glacial maximum. In: Palacios, D., Hughes, P.D., García-Ruiz, J.M., Andrés, N. (Eds.), European Glacial Landscapes. Maximum Extent of Glaciations. Elsevier, pp. 283–294. https://doi.org/10.1016/B978-0-12-823498-3.00008-X. Chap. 39.
Jrbashyan, R.T., Ghukasyan, Y.G., Karapetyan, S.G., Mnatsakanyan, A. Kh, Navasardyan, G. Kh, Gevorgyan, H.P., 2012. Types of volcanic eruptions and forms of manifestation of the late-collision on-land volcanism in Armenia. Arm. Natl. Acad. Sci. Inst. Geol. Sci. Earth Sciences 3, 3–20.
Joannin, S., Ali, A.A., Ollivier, V., Roiron, P., Peyron, O., Chevaux, S., Nahapetyan, S., Tozalakyan, P., Karakhanyan, A., Chataigner, C., 2014. Vegetation, fire and climate history of the Lesser Caucasus: a new Holocene record from Zarishat fen (Armenia). J. Quat. Sci. 29, 70–82.
Johnson, M.D., Clayton, L., 2003. Supraglacial landsystems in lowland terrain. Glacial Landsystems 228–258. https://doi.org/10.4324/9780203784976.
Kalantar, A., 2003. Mount Aragats in history. In: Ashkharabek Kalantar, Materials on Armenian and Urartian History. Civilisations Du Proche-Orient, Hors Serie, vol. 3. Recherches et Publications, Neuchatel, pp. 5–19.
Karakhanyan, A., Abgaryan, Y., 2004. Evidence of historical seismicity and volcanism in the Armenian Highland (from Armenian and other sources). Ann. Geophys. 47 (2/3), 793–810. https://doi.org/10.4401/ag-3335.
Karakhanyan, A., Vernant, P., Doerflinger, E., Avagyan, A., Philip, H., Aslanyan, R., Champollion, C., Arakelyan, S., Collard, P., Baghdasaryan, H., Peyret, M., Davtyan, V., Calais, E., Masson, F., 2013. GPS constraints on continental deformation in the Armenian region and Lesser Caucasus. Tectonophysics 592, 39–45.
Khechoyan, A., Gasparyan, B., 2014. Rock-painting phenomenon in the republic of Armenia. In: Gasparyan, B., Arimura, M. (Eds.), Stone Age of Armenia, A Guide-Book to the Stone Age Archaeology in the Republic of Armenia, Monograph of the JSPS-Bilateral Joint Research Project. Kanazawa University Press, pp. 315–337. Printed in Japan, 2014, ISBN 978-4-9908070-0-9.
Khechoyan, A., Feruglio, V., Gasparyan, B., Chataigner, C., 2007. The rock art of the Mt. Aragats system, rock art in the frame of the cultural heritage of humankind, papers, XXII valcamonica symposium, 18-24 maggio. In: Bloom, M., Giorgi, P., Pietroboni, G. (Eds.), Centro Cogressi Darfo Boario Terme, pp. 247–252.
Kokalj, Ž., Zakšek, K., Oštir, K., 2013. Visualizations of lidar derived relief models. Interpreting archaeological topography: airborne laser scanning. 3D data and ground observation 5, 100–114.
Leontaritis, A.D., 2020. The Late Quaternary Glacial History of Greece. Harokopio University of Athens, p. 195. Doctoral Thesis. https://scholar.google.com/scholar_lookup?title=The%20Late%20Quaternary%20Glacial%20History%20of%20Greece.%20Doctoral%20Thesis&author=A.D.%20Leontaritis&publication_year=2021.
Lindsay, I., Smith, A.T., 2006. A history of archaeology in the republic of Armenia. J. Field Archaeol. 31 (2), 165–184. http://www.jstor.org/stable/40024955.
Lindsay, I., Greene, A.F., Marshall, M.E., Badalyan, R., Cromartie, A., Azatyan, K., Aghikyan, L., Khatchadourian, L., Mkrtchyan, A., Smith, A.T., 2022. The project ArAGATS kasakh valley archaeological survey, Armenia: report of the 2014–2017 seasons. Am. J. Archaeol. 126 (2), 261–303. https://doi.org/10.1086/718333.
Lisiecki, L., Raymo, M., 2005. A Pliocene – Pleistocene stack of 57 globally distributed benthic d18O records. Paleoceanography 20 (1), 17. https://doi.org/10.1029/2004PA001071.
Loveluck, C.P., Tielidze, L.G., Elashvili, M., Kurbatov, A.V., Gadrani, L., Erb-Satullo, N., von Suchodoletz, H., Dan, A., Laermanns, H., Brückner, H., Schlotzhauer, U., Sulava, N., Chagelishvili, R., 2024. Rapid climate change, Integrated human–environment–historical records and societal Resilience in Georgia. Sustainability 16, 7116. https://doi.org/10.3390/su16167116.
López-Moreno, J.I., García-Ruiz, J.M., 2024. Discrepancies in dating the expansion of European glaciers during the last glacial cycle. Geomorphology 471, 109566. https://doi.org/10.1016/j.geomorph.2024.109566.
Lukas, S., 2006. Morphostratigraphic principles in glacier reconstruction – a perspective from the British Younger Dryas. Prog. Phys. Geogr. 30, 719–736. https://doi.org/10.1177/0309133306071955.
Malinsky-Buller, A., Edeltin, L., Ollivier, V., Joannin, S., Peyron, O., Lauer, T., Frahm, E., Brittingham, A., Hren, M.T., Sirdeys, N., Glauberman, P., Adigyozalyan, A., Gasparyan, B., 2024. The environmental and cultural background for the reoccupation of the Armenian Highlands after the Last Glacial Maximum: the contribution of Kalavan 6. J. Archaeol. Sci.: Reports 56, 104540. https://doi.org/10.1016/j.jasrep.2024.104540.
Marrero, S.M., Phillips, F.M., Borchers, B., Lifton, N., Aumer, R., Balco, G., 2016. Cosmogenic nuclide systematics and the CRONUScalc program. Quat. Geochronol. 31, 160–187. https://doi.org/10.1016/j.quageo.2015.09.005.
Menviel, L., Capron, E., Govin, A., Dutton, A., et al., 2019. The penultimate deglaciation: protocol for Paleoclimate Modelling Intercomparison Project (PMIP) phase 4 transient numerical simulations between 140 and 127 ka, version 1.0. Geosci. Model Dev. (GMD) 12, 3649–3685. https://doi.org/10.5194/gmd-12-3649-2019.
Merchel, S., Bremser, W., Alfimov, V., Arnold, M., Aumaître, G., Benedetti, L., Bourlès, D. L., Caffee, M., Fifield, L.K., Finkel, R.C., Freeman, S.P.H.T., Martschini, M., Matsushi, Y., Rood, D.H., Sasa, K., Steier, P., Takahashi, T., Tamari, M., Tims, S.G., Tosaki, Y., Wilcken, K.M., Xu, S., 2011. Ultra-trace analysis of 36Cl by accelerator mass spectrometry: an interlaboratory study. Anal. Bioanal. Chem. 400 (9), 3125–3132. https://link.springer.com/article/10.1007/s00216-011-4979-2.
Mergevosovich, A.A., Yurievich, B.V., Razmikovna, P.G., 2024. Analysis of registration and processing of seismological data in the republic of Armenia from 1991 to 1998. Open Access Library Journal 11, e11409. https://doi.org/10.4236/oalib.1111409.
Mitchell, W.M., 1996. Significance of snowblow in the generation of loch Lomond stadial (younger Dryas) glaciers in the western Pennines, northern England. J. Quat. Sci. 11 (3), 233–248. https://doi.org/10.1002/(SICI)1099-1417(199605/06)11:3<233::AID-JQS240>3.0.CO;2-Q.
Mitchell, S.G., Montgomery, D.R., 2006. Influence of a glacial buzzsaw on the height and morphology of the Cascade Range in central Washington State, USA. Quat. Res. 65, 96–107. https://doi.org/10.1016/j.yqres.2005.08.018.
Mix, A.C., Bard, E., Schneider, R., 2001. Environmental processes of the ice age: land, oceans, glaciers (EPILOG). Quat. Sci. Rev. 20, 627–657. http://refhub.elsevier.com/S0277-3791(15)30119-0/sref99.
Moussavi, M.S., Zoej, M.J.V., Vaziri, F., Sahebi, M.R., Rezaei, Y., 2009. A new glacier inventory of Iran. Ann. Glaciol. 50 (53), 93–103. https://doi.org/10.3189/172756410790595886.
Nadel, D., Bar-Oz, G., Malkinson, D., Spivak, P., Langgut, D., Porat, N., Kechaoyan, A., Nachmias, A., Crater-Gershtein, E., Katinaa, A., Bermatov-Paz, G., Nahapetyan, S., Gasparyan, B., 2015. New insights into desert kites in Armenia: the fringes of the

Ararat Depression. Arabian Archaeol. Epigr. 26 (2), 120–143. https://doi.org/10.1111/aae.12057.
NASA, 2002. ID STS 059-201-95, Gateway to Astronaut Photography ofEarth.
Neill, I., Meliksetian, K., Allen, M.B., Navarsardyan, G., Karapetyan, S., 2013. Pliocene-Quaternary volcanic rocks of NW Armenia: magmatism and lithospheric dynamics within an active orogenic plateau. Lithos 180–181, 200–215. https://doi.org/10.1016/j.lithos.2013.05.005.
Neill, I., Meliksetian, K., Allen, M.B., Navasardyan, G., Kuiper, K., 2015. Petrogenesis of mafic collision zone magmatism: the Armenian sector of the Turkish–Iranian Plateau. Chem. Geol. 403, 24–41.
Nestler, A., Huss, M., Ambartzumian, R., Hambarian, A., 2014. Hydrological implications of covering wind-blown snow accumulations with geotextiles on Mount Aragats, Armenia. Geosciences 4, 73–92. https://doi.org/10.3390/geosciences4030073.
Ocakoğlu, F., Tuncay, E., Hu, H.M., Shen, C.C., 2024. Middle Holocene Göynük landslide (NW Anatolia): geomorphological frame, failure mechanism, and a large (Mw7.9) earthquake trigger from the North Anatolian fault. Geomorphology 463. https://doi.org/10.1016/j.geomorph.2024.109370.
Oliva, M., Palacios, D., Fernández-Fernández, J.M., Rodríguez-Rodríguez, L., García-Ruiz, J.M., Andrés, N., Carrasco, R.M., Pedraza, J., Pérez-Alberti, A., Valcárcel, M., Hughes, P.D., 2019. Late quaternary glacial phases in the Iberian Peninsula. Earth Sci. Rev. 192, 564–600. https://doi.org/10.1016/j.earscirev.2019.03.015.
Oliva, M., Fernández-Fernández, J.M., Palacios, D., 2022. The Iberian mountains: glacial landforms from the last glacial maximum. In: Palacios, D., Hughes, P.D., García-Ruiz, J.M., Andrés, N. (Eds.), European Glacial Landscapes. Elsevier, pp. 473–480. https://doi.org/10.1016/B978-0-12-823498-3.00029-7.
Ollivier, V., Nahapetyan, S., Roiron, P., Gabrielyan, I., Gasparyan, B., Chataigner, C., Joannin, S., Cornée, J.J., Guillou, H., Scaillet, S., Munch, P., Krijgsman, W., 2010. Quaternary volcano-lacustrine patterns and palaeobotanical data in southern Armenia. Quat. Int. 223–224, 312–326. https://doi.org/10.1016/j.quaint.2010.02.008.
Olyphant, G.A., 1977. Topoclimate and the depth of cirque erosion. Geogr. Ann. 59A, 209–213.
Oswald, F., 1906. A Treatise on the Geology of Armenia. University of London.
Paffengol'ts, K.N., Ter-Mesropyan, G.T., 1968. Geology and petrology of the Aragats massif (Armenia). Int. Geol. Rev. 10 (4), 369–385.
Palacios, D., Hughes, P.D., García-Ruiz, J.M., Andrés, N., 2022. The Quaternary ice ages. In: Palacios, D., Hughes, P.D., García-Ruiz, J.M., Andrés, N. (Eds.), European Glacial Landscapes. Maximum Extent of Glaciations. Elsevier, pp. 9–18. https://doi.org/10.1016/B978-0-12-823498-3.00006-6.
Palacios, D., Andrés, N., Hughes, P.D., García-Ruiz, J.M., 2023. Introduction. In: Palacios, D., Hughes, P.D., García-Ruiz, J.M., Andrés, N. (Eds.), European Glacial Landscapes. The Last Deglaciation. Elsevier, pp. 3–9. https://doi.org/10.1016/B978-0-323-91899-2.00034-6.
Pedersen, G.B.M., Grosse, P., Gudmundsson, M.T., 2020. Morphometry of glaciovolcanic edifices from Iceland: types and evolution. Geomorphology 370 (1–19), 107334. https://doi.org/10.1016/j.geomorph.2020.107334.
Pedraza, J., Carrasco, R.M., Domínguez-Villar, D., Villa, J., 2013. Late Pleistocene glacial evolutionary stages in the Gredos mountains (Iberian central system). Quat. Int. 302, 88–100. https://doi.org/10.1016/j.quaint.2012.10.038.
Peterson, J.A., 1968. Cirque morphology and Pleistocene ice formation conditions in Southeastern Australia. Aust. Geogr Stud. 6, 67–83.
Peterson, G., Johnson, M.D., 2018. Hummock corridors in the south-central sector of the Fennoscandian ice sheet, morphometry and pattern. Earth Surf. Process. Landf. 43 (4), 919–929. https://doi.org/10.1002/esp.4294.
Petrosyan, A., Arimura, M., Gasparyan, B., Nahapetyan, S., Chataigner, C., 2014. Early Holocene sites of the republic of Armenia: questions of cultural distribution and chronology. In: Gasparyan, B., Arimura, M. (Eds.), Stone Age of Armenia, A Guidebook to the Stone Age Archaeology in the Republic of Armenia, Monograph of the JSPS-Bilateral Joint Research Project. Kanazawa University Press, pp. 135–159. Printed in Japan, 2014, ISBN 978-4-9908070-0-9.
Petrosyan, A., Arimura, M., Nahapetyan, S., Arakelyan, D., Gasparyan, B., 2021. A step Forward to the Neolithization: early Holocene sites of the republic of Armenia. In: Avetisyan, P., Bobokhyan, A. (Eds.), Archaeology of Armenia in Regional Context". Proceedings of the International Conference Dedicated to the 60th Anniversary of the Institute of Archaeology and Ethnography Held on July 9-11, 2019. Publishing House of the Institute of Archaeology and Ethnography, Yerevan, pp. 26–41. ISBN 978-9939-886-04-6.
Preusser, F., 2004. Towards a chronology of the late Pleistocene in the northern alpine foreland. Boreas 33, 195–210. https://doi.org/10.1111/j.1502-3885.2004.tb01141.x.
Railsback, L.B., Gibbard, P.L., Head, M.J., Voarintsoa, N.R.G., Toucanne, S., 2015. An optimized scheme of lettered marine isotope substages for the last 1.0 million years, and the climatostratigraphic nature of isotope stages and substages. Quat. Sci. Rev. 111, 94–106. https://doi.org/10.1016/j.quascirev.2015.01.012.
Rasmussen, S.O., Bigler, M., Blockley, S.P., Blunier, T., Buchardt, S.L., Clausen, H.B., Winstrup, M., 2014. A stratigraphic framework for abrupt climatic changes during the Last Glacial period based on three synchronized Greenland ice-core records: refining and extending the INTIMATE event stratigraphy. Quat. Sci. Rev. 106, 14–28. https://doi.org/10.1016/j.quascirev.2014.09.007.
Reber, R., Akçar, N., Yesilyurt, S., Yavuz, V., Tikhomirov, D., Kubik, P.W., Schlüchter, C., 2014. Glacier advances in northeastern Turkey before and during the global last glacial maximum. Quat. Sci. Rev. 101, 177–192.
Reber, R., Akçar, N., Tikhomirov, D., Yesilyurt, S., Vockenhuber, C., Yavuz, V., Ivy-Ochs, S., Schlüchter, C., 2022. LGM glaciations in the northeastern Anatolian mountains: new insights. Geosciences 12. https://doi.org/10.3390/geosciences12070257.
Revaz, K., Koba, K., Kukuri, T., Giorgi, C., 2018. Ancient glaciation of the Caucasus. Open J. Geol. 8, 56–64. https://doi.org/10.4236/ojg.2018.81004.
Rex, C.L., Staff, R.A., Toney, J.L., Pearson, E., Francke, A., Saito-Kato, M., Nakagawa, T., 2024. Novel observations of east Asian summer Monsoon evolution during glacial termination II from lake Suigetsu, Japan. Down Earth. https://doi.org/10.31223/X5310P.
Ritz, J.F., Avagyan, A., Mkrtchyan, M., Nazari, H., Blard, P.H., Karakhanian, A., Philip, H., Balescu, S., Mahan, S., Huot, S., Münch, P., Lamothe, M., 2016. Active tectonics within the NW and SE extensions of the Pambak-Sevan-Syunik fault: implications for the present geodynamics of Armenia. Quat. Int. 395, 61–78.
Rudolph, E.M., Hedding, D.H., Nel, W., 2021. The glacial geomorphology of sub-Antarctic Marion Island. J. Maps 17 (2), 313–324. https://doi.org/10.1080/17445647.2021.1931970.
Samolczyk, M., Osborn, G., Menounos, B., Clark, D., Davis, P.T., Clague, J.J., Koch, J., 2024. Glacier fluctuation chronology since the latest Pleistocene at Mount Rainier, Washington, USA. Quat. Res. 119, 65–85. https://doi.org/10.1017/qua.2023.63.
Sanders, J.W., Cuffey, K.M., MacGregor, K.R., Collins, B.D., 2013. The sediment budget of an alpine cirque. Geol. Soc. Am. Bull. 125, 229–248.
Sapelko, T.V., Boynagryan, V.R., Naumenko, M.A., Sevastyanov, D.V., Gabrielyan, I.G., Piloyan, A.S., Margaryan, L.A., Aleksandrin, M.Y., Terekhov, A.V., 2019. First Multy-Proxy studies of high-mountain lakes in Armenia: preliminary results. Geography, Environment, Sustainability 12 (4), 272–284. https://doi.org/10.24057/2071-9388-2019-87.
Sarikaya, M.A., Çiner, A., Zreda, M., 2011. Quaternary glaciations of Turkey. In: Ehlers, J., Gibbard, P.L., Hughes, P.D. (Eds.), Quaternary Glaciations - Extent and Chronology, 15, Developments in Quaternary Science. Elsevier Publications, Amsterdam, pp. 393–403. https://doi.org/10.1016/B978-0-444-53447-7.00030-1.
Sarikaya, M.A., Çiner, A., Haybat, H., Zreda, M., 2014. An early advance of glaciers on Mount Akdağ, SW Turkey, before the global Last Glacial Maximum; insights from cosmogenic nuclides and glacier modeling. Quat. Sci. Rev. 88, 96–109. https://doi.org/10.1016/j.quascirev.2014.01.016.
Sarikaya, M.A., Candaş, A., Ege, I., Wilcken, K.M., 2025. Geochronology and ice-flow modelling of the Late Quaternary glaciers on Mt. Soğanlı, Türkiye. J. Quat. Sci. 40 (1), 71–85. https://doi.org/10.1002/jqs.3660.
Schaefer, J.M., Denton, G.H., Barrell, D.J., Ivy-Ochs, S., Kubik, P.W., Andersen, B.G., Phillips, F.M., Lowell, T.V., Schluchter, C., 2006. Near-synchronous interhemispheric termination of the last glacial maximum in mid-latitudes. Science 312 (5779), 1510–1513. https://doi.org/10.1126/science.1122872.
Schimmelpfennig, I., Benedetti, L., Finkel, R., Pik, R., Blard, P.H., Bourlès, D., Burnard, P., Williams, A., 2009. Sources of in situ ^{36}Cl in basaltic rocks. Implications for calibration of production rates. Quatern. Geochronol. 4, 441–461. https://doi.org/10.1016/j.quageo.2009.06.003.
Schimmelpfennig, I., Benedetti, L., Garreta, V., Pik, R., Blard, P.H., Burnard, P., Bourlès, D., Finkel, R., Ammon, K., Dunai, T., 2011. Calibration of cosmogenic ^{36}Cl production rates from Ca and K spallation in lava flows from Mt. Etna (38°N, Italy) and Payun. Matru (36°S, Argentina). Geochem. Cosmochim. Acta 75, 2611–2632. https://doi.org/10.1016/j.gca.2011.02.013.
Schimmelpfennig, I., Schaefer, J.M., Putnam, A.E., Koffman, T., Benedetti, L., Ivy-Ochs, S., , ASTER Team, Schlüchter, C., 2014. ^{36}Cl production rate from K-spallation in the European Alps (Chironico landslide, Switzerland). J. Quat. Sci. 29, 407–413. https://doi.org/10.1002/jqs.2720.
Seijmonsbergen, A.C., 2013. The modern geomorphological map. In: Switzer, A.D., Kennedy, D.M. (Eds.), Methods in Geomorphology, of Treatise on Geomorphology, cap 4, 14. Elsevier, pp. 35–52. https://doi.org/10.1016/B978-0-12-374739-6.00371-7.
Sevastyanov, D.V., Sapelko, T.V., Naumenko, M.A., Boynagryan, V.R., 2021. The rhythm of natural processes in the area of the Aragats Massif (Armenia) according to the Umroi Lake study data. Lomonosov Geography Journal (1), 16–26 (In Russ.).
Shackleton, N.J., 1969. The last interglacial in the marine and terrestrial record. Proc. R. Soc. Lond. Series B 174 (1034), 135–154.
Shalaeva, E.A., Trifonov, V.G., Trikhunkov, Y.I., Titov, V.V., Avagyan, A.V., Sahakyan, L. H., Simakova, A.N., Frolov, P.D., Sokolov, S.A., Vasilyeva, M.A., Bachmanov, D.M., Ovakymyan, G.M., 2023. The neotectonics and geological structure of the sevan intermountain basin (Armenia): new structural and palaeontologic data. Geotectonics 57 (4), 446–459.
Sherriff, J.E., Wilkinson, K.N., Adler, D.S., Arakelyan, D., Beverly, E.J., Blockley, S.P.E., Gasparyan, B., Mark, D.F., Meliksetyan, Kh, Nahapetyan, S., Preece, K.J., Timms, R. G.O., 2019. Pleistocene volcanism and the geomorphological record of the Hrazdan valley, central Armenia linking landscape dynamics and the Palaeolithic record. Quat. Sci. Rev. 226, 1–26. https://doi.org/10.1016/j.quascirev.2019.105994, 105994.
Sherriff, J.E., Wilkinson, K.N., Harding, P., Hawkins, H., Timms, R.G.O., Adler, D.S., Beverly, E.J., Blockley, S.P.E., Gasparyan, B., Manning, C.J., Mark, D., Nahapetyan, S., Preece, K.J., 2021. Middle Pleistocene environments, landscapes and tephrostratigraphy of the Armenian highlands: evidence from Bird Farm 1, Hrazdan valley. J. Quat. Sci. 1–22. https://doi.org/10.1002/jqs.3370, 2021.
Sherriff, J.E., Petrosyan, A., Rogall, D., Nora, D., Frahm, E., Lauer, T., Karambaglidis, T., Knul, M.V., Vettese, D., Arakelyan, D., Gur-Arieh, S., Vidal-Matutano, P., Morales, J., Fewlass, H., Blockley, S.P.E., Timms, R., Adigyozalyan, A., Haydosyan, H., Glauberman, P., Gasparyan, B., Malinsky-Buller, A., 2024. Palaeoenvironmental and chronological context of hominin occupations of the Armenian Highlands during MIS 3: evidence from Ararat-1 cave. Quaternary Science Advances 13, 1–19. https://doi.org/10.1016/j.qsa.2023.100122, 100122.
Şimşek, M., Öztürk, M.Z., Yeşilyurt, S., Utlu, M., 2023. Morphometric characteristics and paleogeographic implication of glacial cirques in Eastern Black Sea Mountains (Türkiye). Geomorphology 441. https://doi.org/10.1016/j.geomorph.2023.108889.

Smith, M.J., Rose, J., Booth, S., 2006. Geomorphological mapping of glacial landforms from remotely sensed data: an evaluation of the principal data sources and an assessment of their quality. Geomorphology 76 (1–2), 148–165. https://doi.org/10.1016/j.geomorph.2005.11.001.

Solomina, O., Bushueva, I., Dolgova, E., Jomelli, V., Alexandrin, M., Mikhalenko, V., Matskovsky, V., 2016. Glacier variations in the Northern Caucasus compared to climatic reconstructions over the past millennium. Glob. Planet. Change 140, 28-50. https://doi.org/10.1016/j.gloplacha.2016.02.008.

Solomina, O.N., Alexandrovskiy, A.L., Zazovskaya, E.P., Konstantinov, E.A., Shishkov, V. A., Kuderina, T.M., Bushueva, I.S., 2022. Late-holocene advances of the greater Azau glacier (Elbrus area, northern Caucasus) revealed by ^{14}C dating of paleosols. Holocene 32, 468–481. https://doi.org/10.1177/09596836221074029.

Soteres, R.L., Peltier, C., Kaplan, M.R., Sagredo, E.A., 2020. Glacial geomorphology of the strait of Magellan ice lobe, southernmost Patagonia, south America. J. Maps 16 (2), 299–312. https://doi.org/10.1080/17445647.2020.1736197.

Spagnolo, M., Pellitero, R., Barr, I.D., Ely, J.C., Pellicer, X.M., Rea, B.R., 2017. ACME, a GIS tool for Automated cirque Metric extraction. Geomorphology 278, 280–286. https://doi.org/10.1016/j.geomorph.2016.11.018.

Stockhecke, M., Timmermann, A., Kipfer, R., Haug, G.H., Kwiecien, O., Friedrich, T., Menviel, L., Litt, T., Pickarski, N., Anselmetti, F.S., 2016. Millennial to orbital-scale variations of drought intensity in the Eastern Mediterranean. Quat. Sci. Rev. 133, 77–95. https://doi.org/10.1016/j.quascirev.2015.12.016.

Stokes, C.R., Gurney, S.D., Shahgedanova, M., Popovnin, V., 2006. Late-20th-century changes in glacier extent in the Caucasus Mountains, Russia/Georgia. J. Glaciol. 52, 99–109. https://doi.org/10.3189/172756506781828827.

Stone, J., 2000. Air pressure and cosmogenic isotope production. J. Geophys. Res. 105, 23753–23760. https://doi.org/10.1029/2000JB900181.

Stone, J.O., Fifield, K., Vasconcelos, P., 2005. Terrestrial chlorine-36 production from spallation of iron. In: Abstract of 10th International Conference on Accelerator Mass Spectrometry. Berkeley California.

Stroeven, A.P., Fabel, D., Harbor, J.M., Fink, D., Caffee, M.W., Dahlgren, T., 2011. Importance of sampling across an assemblage of glacial landforms for interpreting cosmogenic ages of deglaciation. Quat. Res. 76 (1), 148–156. https://doi.org/10.1016/j.yqres.2011.04.004.

Štular, B., Kokalj, Ž., Oštir, K., Nuninger, L., 2012. Visualization of lidar-derived relief models for detection of archaeological features. J. Archaeol. Sci. 39 (11), 3354–3360.

Sugden, D.E., John, B.S., 1976. Glaciers and Landscape: A Geomorphological Approach. Edward Arnold, London, p. 376, 1976.

Tielidze, L.G., 2017. Late Pleistocene and Holocene glacier extent in the Georgian Caucasus. Open J. Geol. 7, 517–532. https://doi.org/10.4236/ojg.2017.74036.

Tielidze, L.G., Solomina, O.N., Jomelli, V., Dolgova, E.A., Bushueva, I.S., Mikhalenko, V. N., Brauche, R., 2020. Change of chalaati glacier (Georgian Caucasus) since the little ice age based on dendrochronological and Beryllium-10 data. Ice and Snow 60 (3), 453–470. https://doi.org/10.31857/S2076673420030052.

Tielidze, L.G., Wheate, R.D., 2018. The greater Caucasus glacier inventory (Russia, Georgia and Azerbaijan). Cryosphere 12, 81–94. https://doi.org/10.5194/tc-12-81-2018.

Tielidze, L.G., Charton, J., Jomelli, V., Solomina, O.N., 2023. Glacial geomorphology of the notsarula and Chanchakhi river valleys, Georgian Caucasus. J. Maps 19 (1). https://doi.org/10.1080/17445647.2023.2261490.

Trifonov, V.G., Shalaeva, E.A., Saakyan, L.K., Bachmanov, D.M., Lebedev, V.A., Trikhunkov, Y.I., Simakova, A.N., Avagyan, A.V., Tesakov, A.S., Frolov, P.D., Lyubin, V.P., Belyaeva, E.V., Latyshev, A.V., Ozherelyev, D.V., Kolesnichenko, A.A., 2017. Quaternary tectonics of recent basins in northwestern Armenia. Geotectonics 51, 499–519.

Tsereteli, N., Tibaldi, A., Alania, V., Gventsadse, A., Enukidze, O., Varazanashvili, O., Müller, B.I.R., 2016. Active tectonics of central-western Caucasus, Georgia. Tectonophysics 691, 328–344. https://doi.org/10.1016/j.tecto.2016.10.025.

Tsomaya, V.Sh, Vanesyan, V.K., Akopyan, G.V., 1983. Modern glaciation of Mount Aragats. Izvestiya AN Arm. Ssr. Earth Sci. 2, 44–51 (In Russ.).

Turnbull, J.M., Davies, T.R.H., 2006. A mass movement origin for cirques. Earth Surf. Process. Landf. 31, 1129–1148.

Turu, V., 2023. Asymmetries within the pyrenees and correlation across the westernmost European mountain ranges. In: Mid-Late Pleistocene Glacial Dynamics in the Valira Valleys (Principality of Andorra). Barcelona Univ, Barcelona, Spain. Ph.D. Thesis. https://diposit.ub.edu/dspace/handle/2445/202680.

Unwin, D.J., 1973. The distribution and orientation of corries in northern Snowdonia, Wales. Trans. Inst. Br. Geogr. (58), 85–97.

van Hinsbergen, D.J.J., Gürer, D., Koç, K., Lom, N., 2024. Shortening and extrusion in the east anatolian plateau: how was Neogene Arabia-Eurasia convergence tectonically accommodated? Earth Planet Sci. Lett. 641, 118827. https://doi.org/10.1016/j.epsl.2024.118827.

Vieira, G., Palacios, D., Andrés, N., Mora, C., Váazquez-Salem, L., Woronko, B., Soncco, C., Úbeda, J., Goyanes, G., 2021. Penultimate Glacial Cycle glacier extent in the Iberian Peninsula: new evidence from the Serra da Estrela (Central System, Portugal). Geomorphology 388, 107781. https://doi.org/10.1016/j.geomorph.2021.107781.

von Suchodoletz, H., Gärtner, A., Zielhofer, C., Faust, D., 2018. Eemian and post-Eemian fluvial dynamics in the Lesser Caucasus. Quat. Sci. Rev. 191, 189–203. https://doi.org/10.1016/j.quascirev.2018.05.012.

Wegwerth, A., Plessen, B., Kleinhanns, I.C., Arz, H.W., 2021. Black Sea hydroclimate and coupled hydrology was strongly controlled by high-latitude glacial climate dynamics. Commun. Earth Environ. 2. https://doi.org/10.1038/s43247-021-00129-3.

Westaway, R., 1990. Seismicity and tectonic deformation rate in Soviet Armenia: implications for local earthquake hazard and evolution of adjacent regions. Tectonics 9 (3), 477–503.

Whalley, W.B., 2024. Remote sensing and landsystems in the mountain domain: FAIR data accessibility and landform identification in the digital Earth. Remote Sens. 16, 3348. https://doi.org/10.3390/rs16173348.

White, W.A., 1970. Erosion of cirques. J. Geol. 78, 123–126.

Wolf, D., Lomax, J., Sahakyan, L., Hovakimyan, H., Profe, J., Schulte, P., von Suchodoletz, H., Richter, C., Hambach, U., Fuchs, M., Faust, D., 2022. Last glacial loess dynamics in the Southern Caucasus (NE-Armenia) and the phenomenon of missing loess deposition during MIS-2. Sci. Rep. 12, 13269. https://doi.org/10.1038/s41598-022-17021-5.

Wolf, A., Baker, J.L., Tjallingii, R., Cai, Y., Osinzev, A., Antonosyan, M., Amano, N., Johnson, K.R., Skiba, V., McCormack, J., Kwiecien, O., Chervyatsova, O.Y., Dublyansky, Y.V., Dbar, R.S., Cheng, H., Martin-Breitenbach, S.F., 2024. Western Caucasus regional hydroclimate controlled by cold-season temperature variability since the Last Glacial Maximum. Commun. Earth Environ. 5, 66. https://doi.org/10.1038/s43247-023-01151-3.

Yavaşli, D.D., Tucker, C.J., Melocik, K.A., 2015. Change in the glacier extent in Turkey during the landsat era. Remote Sens. Environ. 163, 32–41. https://doi.org/10.1016/j.rse.2015.03.002.

Yavuz, E.V., 2014. Antique quarries of marmor troadense (NW Turkey): insights from field mapping and absolute dating. Turk. J. Earth Sci. 23, 495–512. https://doi.org/10.3906/yer-1404-2.

Yokoyama, R., Shirasawa, M., Pike, R.J., 2002. Visualizing topography by openness: a new application of image processing to digital elevation models. Photogramm. Eng. Rem. Sens. 68, 257–265.

Zakšek, K., Oštir, K., Kokalj, Ž., 2011. Sky-view factor as a relief visualization technique. Remote Sens. 3 (2), 398–415. https://doi.org/10.3390/rs3020398.

Zasadni, J., 2007. The little Ice age in the Alps: its record in glacial deposits and rock glacier formation. Studia Geomorphologica Carpato-Balcanica 41, 117–137.

Zhao, H., Zhou, W., Cheng, P., Yu, X., Wu, Y., Shu, P., Xian, F., Du, H., Zhou, J., Zhao, G., Fan, Y., Fu, Y., Dong, G., Lu, X., 2024. Holocene temperature and cold events recorded in arid Central Asian peatlands. Quat. Sci. Rev. 328, 108538. https://doi.org/10.1016/j.quascirev.2024.108538.